Draft version July 24, 2013
Preprint typeset using LaTeX style emulateapj v. 11/10/09

Mowgli: INTERACTIVE MANUAL MODELING OF STRONG GRAVITATIONAL LENSES

Philip S. Naudus[1,2], Philip J. Marshall[3,4], and John F. Wallin[1,5]

Draft version July 24, 2013

ABSTRACT

We present Mowgli, a web-based tool for modeling gravitational lens systems designed to be used by citizen scientists when analyzing candidates selected from very large imaging surveys. The lens and source models are constructed manually, via a cursor-controlled Java applet; multiple mass components, image masks and source brightness distributions can be placed directly on an astronomical image of the lensing system, and then manipulated. The predicted lensed and PSF-convolved images are generated in real time, as are the caustics and critical curves of the lens model. The lens model comprises any number of elliptically-symmetric singular isothermal mass distributions, while the sources are modeled as having elliptically-symmetric Gaussian surface brightness distributions. The model parameters are optimized manually by the user, with reference to both a display of the image residuals and a quantified goodness of fit statistic. An experienced user can typically find a reasonable model in a few minutes, with refinements to improve the accuracy taking longer. Automated optimization is also provided, to refine the approximate models found by hand. We demonstrate the applet's operation by modeling the twenty candidate lens systems identified in the SDSS imaging survey as part of the CASSOWARY project. We confirm, by modeling, 12 of the 20 systems are gravitational lenses, 6 are likely to be lenses, and 2 systems cannot be easily modeled as gravitational lenses. We measure the physical Einstein radii of the CASSOWARY lenses (at redshift 0.3–0.6) and find them to be comparable (10–50 kpc) to those of group-scale lenses found at higher redshift in higher resolution imaging surveys.

Subject headings: gravitational lensing — methods: data analysis

1. INTRODUCTION

Strong gravitational lenses – massive objects, such as galaxies or clusters of galaxies, that cause multiple-imaging of objects lying directly behind them – have a wide range of applications in astrophysics and cosmology (see *e.g.* Schneider et al. 2006, for an introduction). Notably, lenses have been used very successfully in recent years to allow us to measure the distribution of dark and luminous matter in galaxies (*e.g.* Gavazzi et al. 2007; Koopmans et al. 2009), groups (*e.g.* Limousin et al. 2009) and clusters (*e.g.* Bradač et al. 2006; Limousin et al. 2008), and to provide a magnified view of the high redshift universe (*e.g.* Pettini et al. 2002; Stark et al. 2008; Swinbank et al. 2009), including populations of galaxies not easily studied by ordinary means (*e.g.* Blain et al. 1999; Stark et al. 2007; Bradač et al. 2009).

Searches for gravitational lenses typically have two stages, namely the selection of objects that could be lenses ("lens candidates"), and then the verification (or rejection) of those candidates by follow-up observation. There is, inevitably, a trade-off between completeness and efficiency in the candidate selection stage. For example, in the CLASS survey, flat-spectrum radio sources were selected that appeared as extended, not point-like, objects in the radio maps of the FIRST survey (Browne et al. 2003). Some 16,500 of these were observed in a VLA snapshot campaign and found to have gravitational lens image morphologies, leading to a complete sample of 22 systems. In contrast, the SLACS team selected just 141 luminous red galaxies from the SDSS spectroscopic survey whose spectra showed clear evidence of there being a higher redshift emission line galaxy in the same fiber aperture; HST snapshot follow-up of these revealed 85 of them to be certain galaxy-scale gravitational lenses (Bolton et al. 2006; Auger et al. 2009).

A promising way to find useful gravitational lenses in greater numbers is to search optical images directly. Sources are plentiful in the visible wavebands, where faint blue galaxies appear on the sky at a density of ~ 100 per square arcminute (Benítez et al. 2004, *e.g.*); these sources can in principle be separated from the intervening lens galaxy light by their color and the image morphology (see *e.g.* Moustakas et al. 2007; Cabanac et al. 2007; Faure et al. 2008; Hennawi et al. 2008; Jackson 2008; Marshall et al. 2009). Lens-finding in optical images has a long history, stretching back to the first lensed quasar (Walsh et al. 1979) and the first giant cluster arcs (Fort 1987) – they were discovered as soon as enough sky was surveyed at sufficient resolution. This remains perhaps the most compelling reason to consider lens-searching in this way: high resolution optical imaging surveys covering very wide areas are being carried out and planned for the coming decade, with very different primary science (such as weak lensing, supernova discovery, galaxy photometric redshift surveys, asteroid tracking and so on) in mind. Between them, the CFHTLS ($\sim 170\mathrm{deg}^2$), SDSS I-III ($\sim 10,000\mathrm{deg}^2$), PS1 ($\sim 30,000\mathrm{deg}^2$), DES ($\sim 5,000\mathrm{deg}^2$) and LSST ($\sim 20,000\mathrm{deg}^2$) aim to im-

[1] Department of Computational and Data Science, George Mason University, Fairfax, VA 20030, USA
[2] Department of Physics & Astronomy, Rutgers University, Piscataway, NJ 08854, USA
[3] KIPAC, P.O. Box 20450, MS29, Stanford, CA 94309, USA
[4] Department of Physics, University of Oxford, Keble Road, Oxford, OX1 3RH, UK
[5] Computational Science Program & Department of Physics, Middle Tennessee State University, Fairfax, VA 20030, USA

age the entire sky at sub-arcsecond image quality, revealing many thousands of well-resolved multiple image systems (see *e.g.* Oguri & Marshall 2010; LSST Science Collaborations et al. 2009).

One of the biggest challenges when exploiting these rich new datasets to find large numbers of new gravitational lenses will be increasing the efficiency of the process. Simple database selections based on object (either lens galaxy or lensed image) color and morphology typically produce samples that are relatively impure (Allam et al. 2007; Hennawi et al. 2008; Faure et al. 2008). In the case of *simple* lenses, efficiency can be increased by using filters specifically designed to catch the most common characteristic lensed image geometries, albeit at the cost of some completeness (Marshall et al. 2009; Kubo et al. 2009). The more simplistic the lens identification algorithm, the less complete the sample of candidates will be; moreover, it is the simple algorithms that are most likely to fail on the complex lenses, which are of interest for at least some of the science projects discussed above.

Some automated methods do contain a crucial ingredient: a lens model. Indeed, we follow Marshall et al. (2009) and argue that a *necessary condition for an object to be considered a good lens candidate is that its system of images be explained by a gravitational lens model.* Fitting the image data for a candidate system by computer modeling allows objective and quantitative statements to be made about whether or not the system is a gravitational lens or not. However, the process is typically quite CPU-intensive, especially for complex lenses (see e.g. Brewer et al. 2010, for the state of the art). Also, the data have to be carefully masked and the putative lens galaxy light subtracted before the fit, to avoid the fitting algorithms becoming confused by unlensed features in the image (see *e.g.* Bolton et al. 2006). Indeed, fully automated lens identification has not yet been demonstrated for complex lenses.

The model fit condition has, effectively, been applied in all imaging survey lens searches carried out to date, including those based purely on visual inspection of the pre-selected candidates (*e.g.* Moustakas et al. 2007; Jackson 2008). In these searches, an expert inspector carried out a qualitative *mental modeling* of the image data associated with each candidate, including accounting for features in the image that are *not* due to lensing. **The presentation of the image data is very important. Informative color composites can be more readily assessed by an inspector than can a single filter image: both the color scale and the image stretch will likely have been chosen to maximize the visibility of the features of interest in the image. Moreover, such images are usually stored in compressed JPEG format, reducing the data storage and transfer overheads.** Mental modeling is fast because it uses the inspector's own powerful neural network to classify objects based on a (typically) large training set of previously experienced lenses and non-lenses. However, it is labor-intensive – and so may lead to incompleteness and poorly-defined selection functions as inspector fatigue sets in. One solution to this problem is to have many inspectors classify the same sample. Another issue is the reliability of the human classification: are mental models really good enough? If the training set is not large or diverse enough, omissions and mis-identifications will occur. This problem is solved by actually fitting the data, to show that the observed features are consistent with being multiple images of the same source, distorted by a plausible gravitational lens in a plausible way.

In this work, we explore a hybrid approach between computer and mental lens modeling. We introduce and demonstrate a new tool, MOWGLI,[1] for interactively fitting images of candidate gravitational lenses. This web-based Java applet should allow large numbers of lens inspectors, with minimal training, to classify candidate complex lenses by making quantitative *manual models* of them. **As a first step towards this goal, we ask here the following questions: Can approximate lens models be made in a usefully short time, using survey imaging data? How do the estimated lens model parameters and their uncertainties differ when color JPEG "data" are used, instead of single filter FITS images? From models inferred using** MOWGLI**, what can we conclude about the CASSOWARY lens candidates?**

This paper is organised as follows. We first set the scene in Section 2, briefly describing the online citizen science community, making a case for extending their activities to appropriately-supported detailed data modeling. In Section 3, we describe our particular data model, including the gravitational lens itself, but also how we treat the input data. We then describe, in Section 5, how the parameters of this model are manually optimized, presenting the MOWGLI applet. In Section 6, we define our demonstration dataset, the CASSOWARY candidate lens sample, and in Section 7 present our results from manually modeling these systems. We discuss our findings and implications for future work in Section 8 and draw conclusions in Section 9.

2. LENS MODELING BY CITIZEN SCIENTISTS

One way of solving the problems of visual lens-searching is to "crowd-source" them to a large group of volunteer "citizen scientists." One of the largest and most successful of these projects in astronomy is the Zooniverse,[6] perhaps best known for its initial project, Galaxy Zoo. The initial premise of this project was that people, even those with no astronomical training, are better than computers at classifying the morphology of galaxies. In the 3 years since its launch in 2007, more than 250,000 Zoo users classified galaxies; in a single year, participants generated over 60 million classifications (Lintott et al. 2008). More recently, citizen scientists on this site have been involved in detecting solar storms, characterization of lunar terrain, and modeling interacting galaxies. The users of the Zooniverse are members of the public who are motivated by participation in the scientific enterprise and are capable of certain kinds of expert analyses following some training (Raddick et al. 2010).

Encouraged by the successes of Galaxy Zoo (*e.g.* Lintott et al. 2008; Land et al. 2008; Cardamone et al. 2009), we propose that lens identification is a task that can be performed by citizen scientists. In this paper, we describe

[1] MOWGLI is an acronym, for Manually Operated Widget for Gravitational Lens Identification.

[6] `http://zooniverse.org`

a way of providing citizen scientists with this training, enabling them to identify gravitational lenses through image modeling. Rather than their absorbing various treatises on lensing theory and the literature on the various lensing effects, we suggest that it is more important that users learn what gravitational lensing *looks like*, and that this learning is best done by *playing* with an *interactive lensed image modeler*. Moreover, the results of the users' attempts to manually model candidate lenses will contain information about the likelihood of their actually being lenses, allowing the systems to be ranked and rejected. We do not test these suppositions rigorously here, but merely take the first step towards a crowd-sourced gravitational lens search by presenting a tool, "Mowgli," for manually modeling images of gravitational lenses, and demonstrate its use on twenty candidate systems from the SDSS imaging survey, selected by the CASSOWARY project (Belokurov et al. 2007, 2009).

Moreover, we anticipate that Mowgli, which we make available as a web-based Java applet, will also be of use to those in the professional astronomy community working with gravitational lenses. Being able to make a quick model of a gravitational lens is not only useful for assessing its very plausibility; it is also a useful first step in planning further investigations (for example, follow-up spectroscopy of the lensed galaxies), or to find a suitable starting point for a more detailed analysis. The likelihood function associated with complex strong lens image data is not easy to explore; it typically has multiple peaks, with very steep gradients and high skewness. The experience is that the most difficult part of the inference problem is getting close to the global peak; once there, simple optimizers or Markov Chain Monte-Carlo samplers can characterize that peak well, but the majority of the CPU time spent by these automated routines is typically in the initial peak-finding stage. Sophisticated, but time-consuming, sampling techniques are required to solve this problem (Brewer et al. 2010). A human operator can navigate the likelihood function more efficiently, using their experience to recognize the various patterns in the residuals and not being thrown off by temporarily terrible goodness of fit; indeed, cluster strong lens modeling often involves some skilled manual parameter optimization, with conjugate images being identified by trial and error (*e.g.* Kneib et al. 1993; Smith et al. 2001). As part of our demonstration then, we use Mowgli to measure the parameters of the CASSOWARY lenses, and predict the total magnifications they provide.

Although there have been a number of on-line Citizen Science projects, most have focused on the analysis of large data sets. Projects such as Moon Zoo, Galaxy Zoo, and Stardust allowed volunteers to look for anomalies in large sets of images. To date, however, there have been very few Citizen Science projects that engage volunteers in modeling complex systems. One such project in astronomy is the Cosmic Mergers (Holincheck et al. 2010; Wallin et al. 2010); here, the primary challenge in helping volunteers with little training model complex systems is to develop an intuitive interface to the modeling "engine." A secondary challenge is developing ways of combining the results from many volunteers into a better understanding of the parameter space near regions that are close matches to the desired data. Although we have created an intuitive interface suitable for lens identification volunteers, we will not be addressing the second issue of results synthesis in this paper. Instead, we focus on the engine and its interface itself, which we describe in the next two sections.

3. GRAVITATIONAL LENS MODEL

In this section we describe our mathematical model for complex lenses, and the likelihood function of the multi-filter imaging data. This constitutes the inner workings of Mowgli, whose user operation is described in Section 5 below. The lens and source model components are similar to those used by *e.g.* Marshall et al. (2007) and Brewer et al. (2010), as is the image prediction and likelihood function. In several key places, our approach differs from this previous work, and we point these out explicitly as we go.

3.1. *Lens mass model*

We assume that complex gravitational lenses can be well-approximated by a set of $N_{\rm d}$ simple components, whose gravitational potentials can be simply summed. We imagine that each lens galaxy in the field (usually recognizable as an elliptical galaxy of old, "red" stars) has an elliptically-symmetric, centrally concentrated mass distribution associated with it, and that this mass distribution is a mix of stellar matter, and dark matter, which extends to higher radii than the stars. The resulting total density profile is found, in isolated galaxies, to be well approximated by a simple power law of index -2 (see *e.g.* Koopmans et al. 2003). We therefore take each lens component to be one of these "singular isothermal ellipsoid" (SIE) models. The dark matter need not just be associated with the visible light, and we do not, in fact, enforce this: our mass components are free to be positioned anywhere in the field. However, even in groups and clusters, it is usually the case that the overall dark matter halo (required by the observable lensing effects) is centered on one of the galaxies in the cluster (see *e.g.* Bradač et al. 2006, for an extreme example).

Each lens mass component (which we index here with i from 1 to $N_{\rm d}$) has 5 parameters associated with it: its position $(x_{{\rm d},i}, y_{{\rm d},i})$, the axis ratio of the elliptical isodensity contours $q_{{\rm d},i}$, orientation angle $\phi_{{\rm d},i}$ (measured from the x-axis to the major axis of each ellipse), and Einstein radius $R_{{\rm Ein},i}$ (in arcsec). The Einstein radius of a mass component is (approximately) where an Einstein ring would form, if that component was an isolated galaxy – in practice, the nearby mass components will contribute their own lensing effects and the images will not appear at $R_{{\rm Ein},i}$ from the mass component. Since we do not (in general) know the redshifts of the lens and the source, we cannot use the total mass of the component as a parameter: the Einstein radius is the best we can do to describe the lens "strength" of each component in the model.

The angle though which passing light rays would be deflected by each component, $\boldsymbol{\alpha}_i$, can be calculated following Kormann et al. (1994). This deflection angle varies over the field of view – and indeed must be calculated for each pixel of the image. $\boldsymbol{\alpha}_i$ is just the spatial derivative of the lens potential, so the deflection angles for each component can be computed and simply summed together to get the overall deflection caused by the lens. Likewise, the convergence and shear fields for each component (the

second derivatives of the lens potential) can be simply summed, and then combined to compute the magnification of the lens at each point in the image. Although the magnification is infinite on the critical curve, it is not computationally feasible to handle infinitely large values. For this reason, the critical curve is determined by finding the contour along which the magnification exceeds a predetermined threshold. The magnification and deflection fields could be mapped in more detail by computing them at intervals of a fraction of a pixel (as in Marshall et al. 2007); we trade accuracy for computation speed at this point, and work with the smallest grids possible.

3.2. *Lensed Image Prediction*

A light ray arriving from a position $\boldsymbol{\theta} = (\theta_x, \theta_y)$ on the sky was actually emitted from a position $\boldsymbol{\beta} = (\beta_x, \beta_y)$, but has been deflected through $\boldsymbol{\alpha}$: to predict the image of a lensed source, we calculate $\boldsymbol{\beta}$ for every pixel in the image using the lens equation,

$$\boldsymbol{\beta} = \boldsymbol{\theta} - \boldsymbol{\alpha}(\boldsymbol{\theta}), \quad (1)$$

and then look up the value of the surface brightness $I(\boldsymbol{\beta})$ of the background source galaxy at that position (*e.g.* Newbury & Spiteri 2002; Marshall et al. 2007). In practice, we do not *know* what the deflection angle $\boldsymbol{\alpha}(\boldsymbol{\theta})$ is, nor do we *know* what the source galaxy looks like: all we can do is assume a model for the lens and a model for the source, and compare the resulting predicted images with what we actually see – and then vary the parameters of our model to improve the match.

We model the source galaxy as an elliptically-symmetric blob with Gaussian profile. This is a reasonable approximation for the ubiquitous compact faint blue galaxies seen in, for example, the Hubble Deep Field: these galaxies are the most likely sources since they are the most common background objects. In the cases where the source is more complex than this, or if more than one source is required to match the observed system of gravitational arcs, we allow for multiple Gaussian source components. Each of these $N_{\rm s}$ sources has 6 parameters: its position $(x_{{\rm s},j}, y_{{\rm s},j})$, ellipse axis ratio $q_{{\rm s},j}$, orientation angle $\phi_{{\rm s},j}$ (the angle measured in radians from the positive x-axis counter-clockwise to the major axis of the ellipse), its total brightness $F_{{\rm s},j}$, and its half-light radius $R_{{\rm eff},j}$ in arcsec (within which half the total brightness of the galaxy is contained). The total brightness of the unlensed galaxy is the easiest parameter to determine – we describe two ways in which we do this in Section 4.3 below.

4. DATA

MOWGLI **is designed to work with images uploaded in one of two formats, JPEG and FITS. Color JPEGs are highly informative to a human inspector, with the contrast between different types of galaxy made clear by the different hues present, and the JPEG compression acting to suppress noise in the dark background areas. However, the noise properties (pixel value uncertainties) of such images are not representative of the original raw data, which is usually stored in single filter, FITS format data files. In this section we outline the various considerations necessary when working with the candidate image data in general, and JPEG and raw FITS date in particular.**

The example lens systems we consider in this paper come from the SDSS survey,[7] **a ready source of astronomical FITS image data with corresponding JPEG visualisations. However,** MOWGLI **can work with image data from any telescope.**

4.1. *Masking*

In every astronomical image, there will be artifacts which are not present in the predicted image, such as the lens galaxy and background. MOWGLI allows the user to place masks over these pixels in order that they do not count toward the error between the predicted and astronomical images. Masked pixels are ignored when computing the goodness of fit (Section 4.3).

In order to aid the user in masking out background pixels, MOWGLI allows the user to import a "masking image." If the masking image is not grayscale, MOWGLI will convert it to grayscale after importing it. The user is then able to set a threshold– pixels located at the pixels of the masking image which fall below the threshold are masked.

In the models presented in this paper, the SDSS JPEG image mask was used for for both the JPEG and FITS models, in order that the same pixels were masked in both sets of models. In general, each user would make their own mask for their uploaded image.

4.2. *PSF Blurring*

The images predicted by the lensing of our model source components by our model complex lens are those that would be seen by a perfect telescope above the Earth's atmosphere. We need a predicted image that we can compare to our noisy, blurry data – and so we convolve the images described in the previous section by a circularly symmetric Gaussian point spread function (PSF) to approximate the blurring effect of the atmosphere and telescope optics.

For speed, we map this model PSF onto a small pixel grid ($\gtrsim$ 2 full PSF widths across) and perform the convolution integral numerically. The size of this pixel grid depends on the observed image we are working with. For example, a typical resampled SDSS image might have pixels that are 0.3" wide and a PSF of FWHM 1.4" ($\simeq 5$ pixels); the model PSF would then have Gaussian width 0.6" and we would map the model PSF on to a 11×11 pixel grid. This choice was optimised for computation speed.

If the user imports a FITS image and the PSFWID header keyword exists, the PSF is set to the value in the header. For SDSS FITS images, PSFWID is the FWHM of the PSF in arcseconds, as determined using a double-Gaussian fit. If the user imports a JPEG image or a FITS image without the PSFWID header, the PSF defaults to 1.4". The PSF FWHM may be edited by the user at any time.

4.3. *Measuring goodness of fit*

[7] `http://skyserver.sdss.org/public/en/tools/chart/navi.asp`

Raw image data stored in FITS files have well-understood error properties, allowing us to use correspondingly well-motivated goodness of fit statistics when comparing predicted and observed images. In contrast, the pixel values of a color JPEG are rarely proportional to the astronomical flux received, and the JPEG creation process involves some image smoothing and compression. (This is why we refer to the source's "brightness," rather than its "flux," in Section 3.2 above.) Nevertheless, it is possible to define a statistic to quantify goodness of fit on a *relative* scale. In this section we define the statistics we use to quantify goodness of fit for both JPEG and raw FITS data.

Typically, raw optical astronomical images have pixel values with Gaussian-distributed errors, which motivates the use of the χ^2 statistic as a measure of goodness of fit. We defined the χ^2 of the models fitted to FITS images using:

$$\chi^2 = \sum_i \frac{(F_{\mathrm{obs},i} - F_{\mathrm{pred},i})^2}{\sigma_i^2}, \tag{2}$$

where the σ_i used was the same for all pixels, and determined by computing the standard deviation of the background pixels. These background pixels were determined by applying a simple brightness threshold to the masked pixels.

We are unable to use this same statistic in order to determine the error associated with models fitted to color JPEG images, because we cannot estimate the noise in the image in the same way. In JPEG-filtered images, much of the original background noise is smoothed away. This leads to an artificially small mean square residual pixel value. Moreover, any remaining background is likely to be quite different in each filter. Given the unknown, and difficult to estimate, pixel error, we are prevented from estimating a meaningful absolute goodness of fit. Instead, we define a simple relative statistic $\hat{\chi}^2$ for each channel:

$$\hat{\chi}^2 = \frac{\sum_i (F_{\mathrm{obs},i} - F_{\mathrm{pred},i})^2}{\sum_i F_{\mathrm{obs},i}^2}. \tag{3}$$

This quantity compares the mean squared pixel value in the residual image with the mean squared pixel value in the data image: if $\hat{\chi}^2 = 0.05$, then the model has accounted for 95% of the features in the image. We then use the average of $\hat{\chi}^2$ over the red, green and blue image channels:

$$\hat{\chi}^2_{\mathrm{tot}} = \frac{1}{3}\sum_j \hat{\chi}^2_j. \tag{4}$$

We compute parameter uncertainties by varying each parameter separately until, for FITS images, the χ^2 value increases by $\delta_{\mathbf{FITS}} = 1$. The quoted uncertainties are symmetrized, by exploring χ^2 in both directions and averaging the two results. If a parameter is increased significantly without a significant change in χ^2, the uncertainty of the parameter is assumed to be infinite. For instance, if the ellipticity of a source is small, varying the rotation will result in little to no change of the modeled arcs, resulting in an infinite uncertainty in the rotation.

We note that $\delta_{\mathbf{FITS}}$ will not, in general, be equal to $\delta_{\mathbf{JPEG}}$ for JPEG images, due to the significant differences between JPEG and FITS images. In Section 7.3 below, we calibrate the JPEG-fitted parameter uncertainties against the FITS-fitted parameter uncertainties, for the CASSOWARY sample SDSS data, finding an approximately linear relationship between them.

5. PARAMETER SPACE EXPLORATION

The data model described in the previous section can be thought of as a black box, taking a list of model parameter values as input and producing a predicted image and its associated chi-squared value as output. The next task is to optimize this model, varying the parameters to decrease the value of the chi-squared misfit statistic and (ultimately) find the best-fitting models.

In our approach, the user varies the parameters "by hand," manipulating the elements of the model directly via a graphical representation of it. Figure 0 shows Mowgli in operation, as a user would see it on their web browser. As the model is altered, the predicted and residual images are computed and the display updated in real time, allowing the user to quickly see the results of their manipulations, and quickly learn what makes a good model and what does not. Key to this is an appreciation of how the position of the source relative to the caustic curves influences the system of multiple images that are produced: this is very difficult to program, but is a straightforward pattern recognition task for a human operator. For this reason we continually update the critical curves and caustics in real time. Details of the modeling procedure we use with our tool are in Appendix C.

The brightness of the source is the one parameter we determine automatically, using one of two methods, selected via a toggled switch. In the first method, we rescale the source brightness such that the total brightness of the unmasked portions of the astronomical image (in each channel) equals the total brightness of the same portions of the predicted image. This is very stable, in the sense that the predicted image always has comparable visibility to the observed image. In the second method, we rescale the source brightness such that the $\hat{\chi}^2$ value is minimized: this can be done analytically since the predicted image brightness depends linearly on the source brightness, and the observed image is constant. Specifically, we rescale each channel's predicted image by its own factor η where

$$\frac{d}{d\eta}\hat{\chi}^2 \propto 2\eta \sum_i F_{\mathrm{obs},i}F_{\mathrm{pred},i} - 2\eta^2 \sum_i F_{\mathrm{pred},i}^2 \tag{5}$$

$$= 0,$$

$$\longrightarrow \eta = \frac{\sum_i F_{\mathrm{obs},i}F_{\mathrm{pred},i}}{\sum_i F_{\mathrm{pred},i}^2}. \tag{6}$$

η can be computed very quickly, allowing us to adjust the predicted image brightness dynamically as the model is varied. However, when the model predicts the image very badly, the $\hat{\chi}^2$-optimized brightness is forced to be very low. We found that starting with method 1 and then

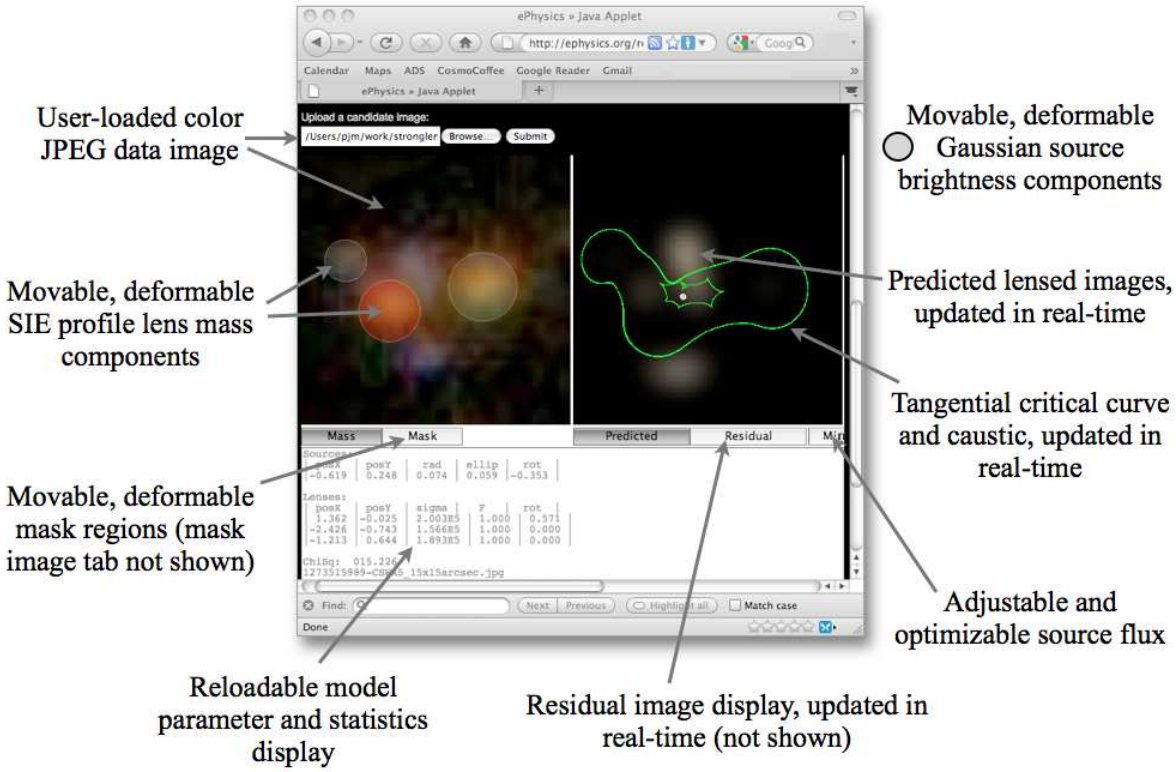

Figure 0. Screenshot of MOWGLI in action. Two image panels show the data image, with either the pixel mask or mass model overlaid on the left, and the predicted image (or the residual image) on the right, with the lens caustics and critical curves, and a representation of the source, overlaid. Underneath the image panels are displayed the model parameters, and the associated chi-squared. Other features to note are the image upload box (top) and buttons for switching between the various viewing options.

changing to method 2 when the fit improved gave the best results.

Once a good model has been found via manual parameter space exploration, the goodness of fit can be automatically optimized. We use the multivariate Nelder-Mead optimizer provided in the Apache Commons library.[8]. We found this step to provide small but valuable refinements to the model when it is indeed already quite good; when run while in a region of low goodness of fit, the result can be a large move to another bad model. This provides some support for the idea that manual exploration is worthwhile: it is difficult to fit lens models to image data automatically, from scratch.

6. THE CASSOWARY SAMPLE

The CASSOWARY sample (Belokurov et al. 2009) is a list of good candidate wide separation gravitational lens systems. The twenty objects used in the present study comprised the 2008 web-only release of this catalog. (The sample continues to grow: by summer 2011, nineteen more objects had been added to the catalog). The CASSOWARY objects were found by systematically searching through the SDSS database for massive ellipticals which appear to be luminous red galaxies (LRGs) with at least two blue companions lying within 6" from the center of the LRG (Belokurov et al. 2009). Candidates were eliminated by constraining the blue companions to fit certain profiles for size and brightness. Each arc was required by the team to have at least two components of comparable magnitude and a bluer color than is typically found in non-lensing systems (Belokurov et al. 2009). The sample is defined, and the candidates' observed properties listed, on the CASSOWARY project website;[9] we reproduce this information in Table 1 for the reader's convenience.

Half of the 20 CASSOWARY systems considered here have been confirmed by some combination of detailed modeling, high resolution imaging, and spectroscopy (Belokurov et al. 2007, 2009; Pettini et al. 2010). Indeed, several were discovered and followed up independently as part of the SDSS Bright Arcs Survey (*e.g.* Lin et al. 2009; Diehl et al. 2009; Kubo et al. 2009, 2010). To date, spectroscopic redshifts have been obtained for the lenses and arcs in CSWA 1–8, CSWA 14 and CSWA 20, showing the blue images to be of background high redshift galaxies, distorted by the lens. The strong lensing –

[8] http://commons.apache.org

[9] `http://www.ast.cam.ac.uk/research/cassowary`

Table 1
The CASSOWARY Lens Candidate Sample

ID	Name	Nickname	$z_{\rm d}$	RA (degrees)	Dec. (degrees)	SDSS phot. ID
CSWA1	SDSS J1148+1930	The Cosmic Horseshoe	0.44[a]	177.13811	19.50089	587742572151374147
CSWA2	SDSS J1038+4849	The Cheshire Cat	0.43[b]	159.67977	48.82195	588013382200131773
CSWA3	SDSS J1240+4509	-	0.27[b]	190.13452	45.15079	588017605222793376
CSWA4	SDSS J0901+1814	-	0.35	135.34322	18.24232	588023046402670876
CSWA5	SDSS J1244+0106	-	0.39[c]	191.21329	1.112080	588848901528223970
CSWA6	SDSS J1206+5142	The Clone	0.42	181.50873	51.70820	588013382206357664
CSWA7	SDSS J1137+4936	-	0.45	174.41690	49.60988	588295841784725744
CSWA8	SDSS J1209+2640	-	0.56	182.34869	26.67960	587741600957333763
CSWA9	SDSS J1227+1725	-	0.37*	186.82809	17.43108	587742902862086260
CSWA10	SDSS J2238+1319	-	0.41	339.63048	13.33218	587730773880078847
CSWA11	SDSS J0800+0812	-	0.31*	120.05442	8.202330	587744873710682762
CSWA12	SDSS J1133+5008	-	0.39[d]	173.30488	50.14447	587732484357095512
CSWA13	SDSS J1237+5533	-	0.41	189.40086	55.56191	587731870173298881
CSWA14	SDSS J1723+3411	-	0.44[e]	260.90071	34.19945	587736980648362708
CSWA15	SDSS J1008+1937	-	0.39	152.24803	19.62124	587742014344265970
CSWA16	SDSS J1111+5308	-	0.40*	167.76458	53.14816	587731868557115670
CSWA17	SDSS J1138+2754	-	0.33*	174.53732	27.90853	587741709956546742
CSWA18	SDSS J1134+2533	-	0.07	173.52810	25.55977	587742191511273514
CSWA19	SDSS J0900+2234	-	0.52*	135.01103	22.56803	587741421640024462
CSWA20	SDSS J1441+1441	-	0.74[f]	220.45482	14.68905	587742611340001632

Notes. Redshifts come from the SDSS public spectroscopic data release DR7 (Abazajian et al. 2009) unless marked as follows: [a]Belokurov et al. (2007), [b]Dye et al. (2008), [c]Christensen et al. (2010), [d]Sand et al. (2005), [e]Kubo et al. (2010), [f]Pettini et al. (2010). An asterisk * indicates a DR7 photometric redshift. The two brightest lens galaxies in CSWA 5, CSWA 15 and CSWA 16 have different redshifts (although for CSWA 16 these are photo-z's) – given here are the arithmetic means of the two values.

i.e. multiple-imaging – nature of the deflectors has been confirmed in some, but not all of these cases, via modeling of follow-up imaging data. Plausible models have therefore not been made for all systems; without such a model, it remains inconclusive whether they really are strong gravitational lenses, *i.e.* causing multiple imaging of a background object.

We analyzed both JPEG and FITS images of the candidates. In most cases, we used the SDSS SkyServer JPEG, as used in the Galaxy Zoo project (Lintott et al. 2008). However, in some cases the low surface brightness arcs did not appear with sufficient contrast: in these cases we made use of the JPEG image provided by the CASSOWARY team on their website, which are in general clearer and brighter than those provided by SDSS, having been individually optimized for visibility. By default, a simple circularly-symmetric Gaussian of FWHM 1.4" was assumed to approximate the SDSS PSF. The field of view of the image must also be specified to allow the JPEG image pixel scale to be computed. **Small "postage stamp" images were excised from the FITS images downloaded from the Skyserver website; these contain the PSFWID keyword and value in their headers, which we used in our Gaussian PSF model. Lastly, we note that all the images in this paper are oriented such that North is up and East is left.**

7. RESULTS

In this section, we first present the results of our MOWGLI modeling of the CASSOWARY sample, providing details of the manual models for each system in turn, and compare them with those in the literature where possible. We then go on to discuss the properties of the sample as a whole.

7.1. *Notes on individual systems*

In Figures 1–20 below, we show two models for each of the CASSOWARY lens candidates. The first model has been optimized to the SDSS multi-filter JPEG data image, while the second model has been optimized to the SDSS FITS image. Each model is accompanied by the predicted lensed image and, corresponding image residual, for our best MOWGLI model. The caustics and critical curves for this lens model are overlaid. By analyzing the Ω values of JPEG and FITS models, no trend was noticed which could indicate that FITS models are better than JPEG models.

CSWA 1: SDSS J1148+1930

This lens candidate, also known as "The Cosmic Horseshoe," is a simple lensing system with a very bright, nearly complete, Einstein ring (Belokurov et al. 2007). These authors showed that CSWA 1 consists of a high-redshift star-forming galaxy being strongly lensed by a massive early-type galaxy (likely the brightest, dominant central member of a group), which, when modeled with a SIE mass distribution was found to have a velocity dispersion parameter of $\sigma_{\rm SIE} \sim 500{\rm kms}^{-1}$ (Dye et al. 2008).

Our MOWGLI lens model, made independently, agrees well with the SIE model presented (Dye et al. 2008), both in terms of Einstein radius and lens ellipticity and orientation. Using the redshifts of the source and lens galaxies presented in Belokurov et al. (2007), we translated our Einstein radius into a velocity dispersion of $\sigma_{\rm SIE} = 506 \pm 5{\rm kms}^{-1}$.

The SIE lens model velocity dispersion is in agreement with the spectroscopic velocity dispersion measured by Belokurov et al. (2007) of $\sigma_{\rm v} = 430 \pm 50{\rm kms}^{-1}$, but significantly higher than the more recent and more ac-

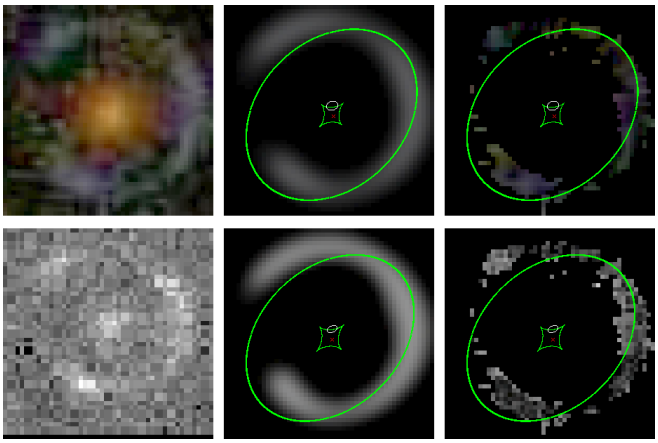

Figure 1. CSWA 1. Top panels: models optimized to SDSS color JPEG image; Bottom panels: models optimized to SDSS FITS image. Left: SDSS data image; Center: model-predicted image; Right: residual image. In this and subsequent figures, the lens model tangential critical curve and caustics are shown overlaid in green, the lens component centroids as red crosses, and the source positions as white circles. The residual image is zero where the data were masked.

curate measurement by Spiniello et al. (2011) of $\sigma_{\rm v} = 351 \pm 10 {\rm kms}^{-1}$. From a more detailed lens model, Dye et al. (2008) found that the density profile *at* the Einstein radius is very close to isothermal; Spiniello et al. (2011) concluded from their lower stellar velocity dispersion that the density profile *within* the Einstein radius must be shallower than isothermal. This illustrates the way that SIE models provide satisfactory fits to lensed image data, even if the actual lens density profile is more complex than this.

The factor of 23 ± 10 magnification that our model predicts is lower than the ~ 50 magnification found by (Belokurov et al. 2007). This is partially a result of our inferred source size being larger: 0.55 arcsec compared to the $\simeq 0.3$ arcsec found by Dye et al. (2008). We found that changing the source size could be offset by increasing the PSF to $1.8''$, although this model has a marginally lower goodness of fit (Ω decreases from 80% to 76%).

CSWA 2: SDSS J1038+4849

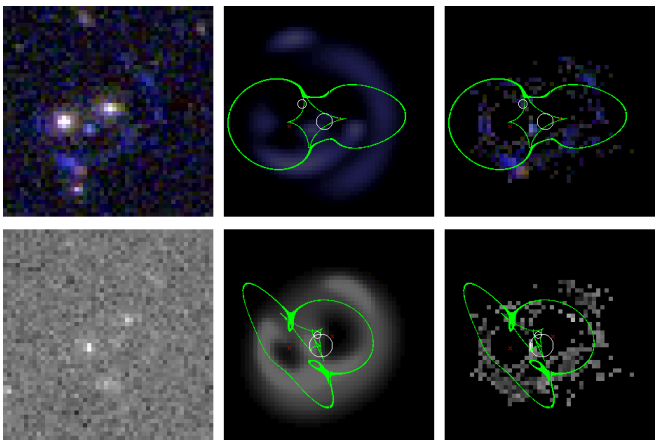

Figure 2. CSWA 2, see Figure 1 for caption.

This confirmed lens, referred to by the CASSOWARY team as "The Cheshire Cat," is a projection of two galaxies (the "eyes" of the Cat) that is lensing two sources, resulting in two bright arcs (Belokurov et al. 2009). The two lens galaxies have similar redshifts ($z = 0.426$ and 0.432), suggesting that our single lens plane assumption might be sufficient. The two sources, however, have quite different redshifts ($z = 0.97$ and $z > 1.4$ Belokurov et al. 2009). We do find a two-component model that predicts images that partially fit the two arc systems, although the residuals are significant ($\Omega = 26\%$). In particular, we predict counter-images in slightly the wrong places. We ascribe some of these difficulties to the multiple lens and source plane redshifts. Nevertheless, our ability to reproduce the brightest and most distorted parts of the arcs supports the strong lensing hypothesis for this system.

Belokurov et al. do not present a lens model, but do give an estimated magnification of the 45 ± 7. This is somewhat higher than our estimate of 17 ± 7, possibly as a consequence of the small discrepancies between models, as discussed above.

CSWA 3: SDSS J1240+4509

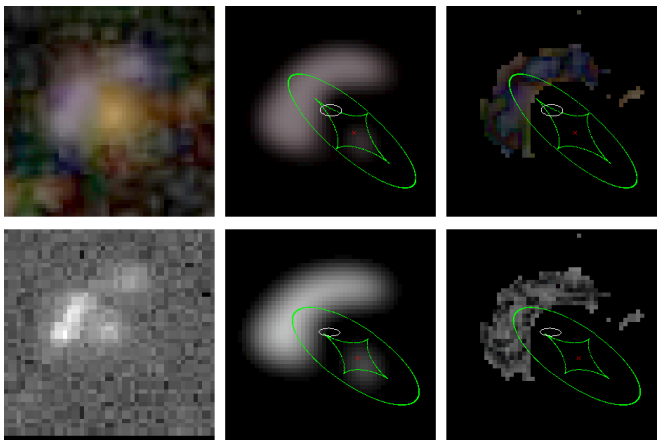

Figure 3. CSWA 3, see Figure 1 for caption.

CSWA 3 consists of a typical star-forming galaxy lensed by a early-type galaxy, and was also discussed by Belokurov et al. (2009). The magnification of our model (7 ± 2) is again rather lower than the $\sim 18 \pm 3$ they found.

The distinctive brightness and curvature of the main arc is very strong evidence for this system being a lens – indeed, our best model predicts the arc to be three merging images. Although our faint residual image indicates good agreement between the predicted and astronomical images, we note that our model does predict a rather high lens ellipticity: the light distribution of the lens is much less elongated. Attempts at modeling this candidate with a lens mass distribution of lower ellipticity were unsuccessful, even when multiple sources were used; these alternative models all feature more prominent counter-arcs which are clearly not present in the data image.

CSWA 4: SDSS J0901+1814

Belokurov et al. (2007) have shown that CSWA 4 consists of a central LRG with many nearby galaxies in the same cluster. Three of these galaxies lie within 10" of the central galaxy. This complicated lens candidate was

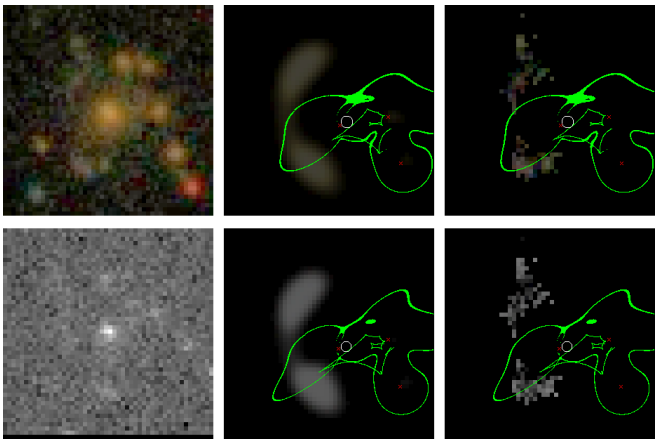

Figure 4. CSWA 4, see Figure 1 for caption.

briefly discussed by Diehl et al. (2009). Independently, we were able to assign mass to each of the 4 central lens galaxies and predict the North-east and South-east arcs, along with a counter-image to the West (slightly offset from its observed position), with a single quadruply-imaged source. The morphology of these arcs is not as well predicted as their position, again suggesting that a more exhaustive search of parameter space is required to obtain a more accurate model of the detailed lens mass structure. In particular, our model predicts the South East arc to be long, composed of 2 merging images, while the observed arc is rather shorter.

CSWA 5: SDSS J1244+0106

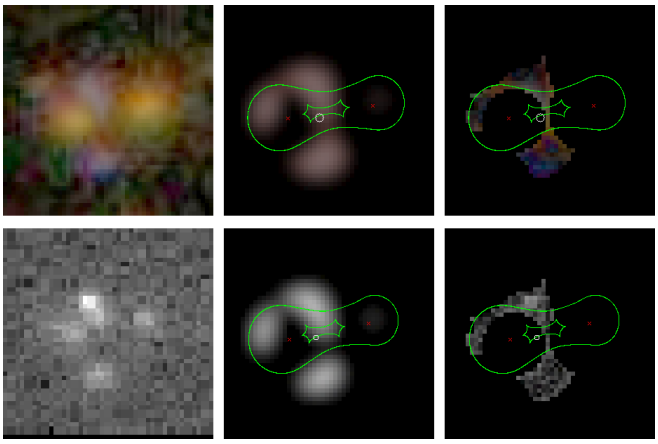

Figure 5. CSWA 5, see Figure 1 for caption.

Belokurov et al. (2007) showed that CSWA 5 consists of a blue star-forming galaxy, lensed by a group (or possibly a line of sight superposition) of red galaxies. As seen in the SDSS survey image, the system consists of two bright red lens galaxies, a faint red satellite nearby, and a bright blue arc and a possible blue counter-image. With slightly higher resolution data, Christensen et al. (2010) found a fourth blue image to the East of the system (not seen in the SDSS image), and suggest that the arc is actually two merging images. They then confirmed that the three images which are roughly aligned vertically have been confirmed to be from the same source, but could not confirm that the fourth, Eastern image is also of this source (Christensen et al. 2010). We find models that reproduce all four images using a single source, by assigning mass to both the bright red galaxies. A better prediction of the position of the fourth image can be obtained by including the faint lens satellite to the North-East as a third mass component.

Christensen et al. (2010) measured the velocity dispersion of the Western lens to be 278 km/s and its redshift to be $z = 0.3877$. (The redshifts and velocity dispersions are expected to be similar for the Eastern lens). Christensen et al. (2010) also determined the redshift of the source to be $z = 1.0686$. Using these redshifts, we determined the velocity dispersion of the Western lens, according to our model, to be 330 ± 10 km/s. Some of this discrepancy is likely due to the difference between the SIE normalisation parameter and the observed aperture spectral velocity dispersion, possibly as a result of a non-isothermal to the mass distribution in the core.

While this paper was being refereed, ?, CG11 published an analysis of CSWA5, finding a very similar binary lens model, with the Einstein radii of the Western and Eastern lenses of 2.01 and 1.75 arcsec respectively. These values are very similar to those we found, but are transposed. ? note that there is significant anticorrelation between these two parameters' error distributions. This is likely to affect both analyses: MOWGLI **fits all the pixels in the image, but with an approximate PSF model, while CG11 assume point-like images. The latter assumption may explain the discrepancy between the** MOWGLI **magnification estimates of 9-13, compared to CG11's 17: the point source approximation will tend to over-estimate the magnification estimate.**

CSWA 6: SDSS J1206+5142

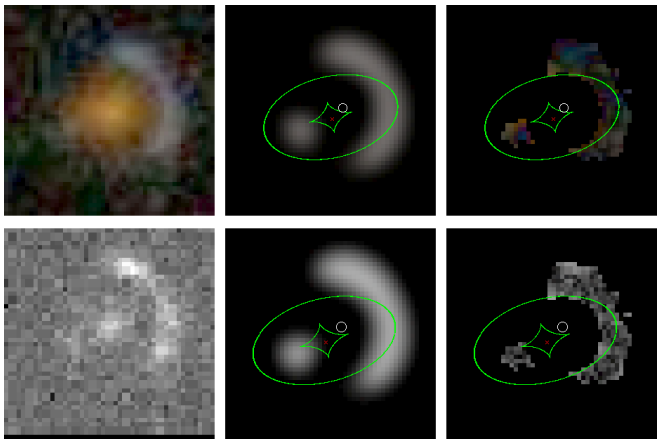

Figure 6. CSWA 6, see Figure 1 for caption.

This lens candidate, referred to in the literature as The Clone, is a simple single-lens system. From follow-up imaging, Lin et al. (2009) determined the Einstein radius to be 3.82 ± 0.03 arcsec and the magnification to be 27 ± 1. We are also able to model the arc and its counter-image, finding an Einstein radius in good agreement (3.8 ± 0.1 arcsec). We again note that the MOWGLI

lens magnification is low compared to the value in the literature, at 14 ± 6, possibly due to the PSF width–source size degeneracy.

CSWA 7: SDSS J1137+4936

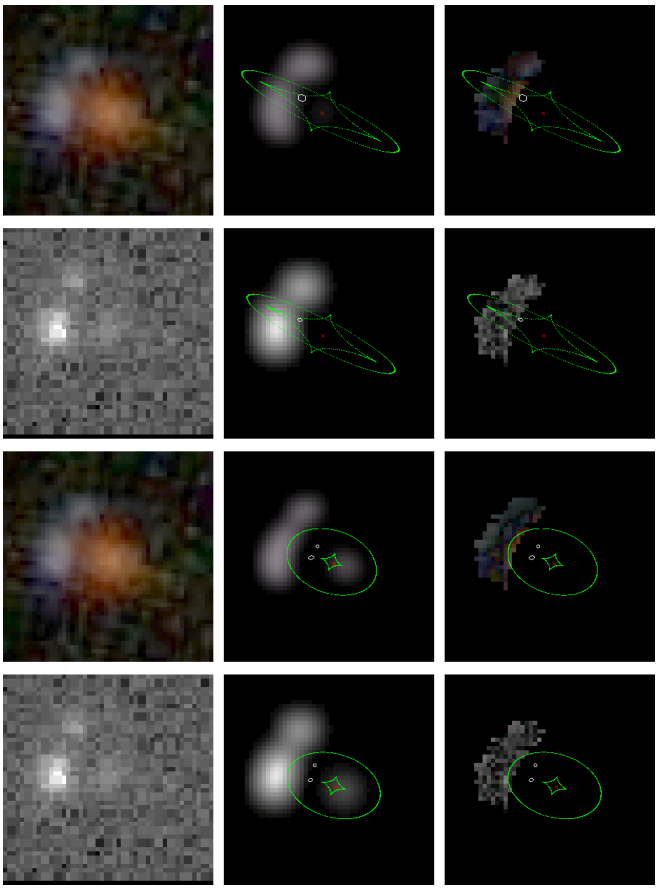

Figure 7. CSWA 7, showing models with one source (top row) and 2 sources (bottom row). Otherwise see Figure 1 for caption.

This lens candidate was selected, followed up and analyzed by Kubo et al. (2009), who determined it to consist of a single lens and two spatially-unresolved sources (the latter piece of information coming from their optical spectroscopy). The brightest blue image component lies at 3.7 arcsec from the putative lens galaxy. For this reason, we present two models of this lens candidate – one (7a) with a single source ($R_{\rm Ein} = 2.6 \pm 0.2$"), and one (7b) with two sources ($R_{\rm Ein} = 2.9 \pm 0.1$").

Although both models have faint residual images, neither of them are ideal. The single-source model predicts a high ellipticity in the lens (see the discussion of CSWA 5), which, compared with the lens galaxy light distribution, seems unlikely. The double-source model has lower ellipticity: instead of predicting one giant arc, it has each of the two distinguishable images coming from a unique source. However, this model predicts quite a bright counter-image not seen in the SDSS image. A third model would have neither source multiply-imaged, but perhaps just brightened and distorted by the gravitational field of what would then be a "weak" lens. The imaging data alone cannot rule this possibility out. As Kubo et al. (2009) point out, spatially-resolved spectroscopy would help in deciding between these two models, as would an independent mass estimate of the lens from a spectroscopic velocity dispersion. Improved imaging to search for the required counter-image would perhaps make the most compelling case for this candidate.

CSWA 8: SDSS J1209+2640

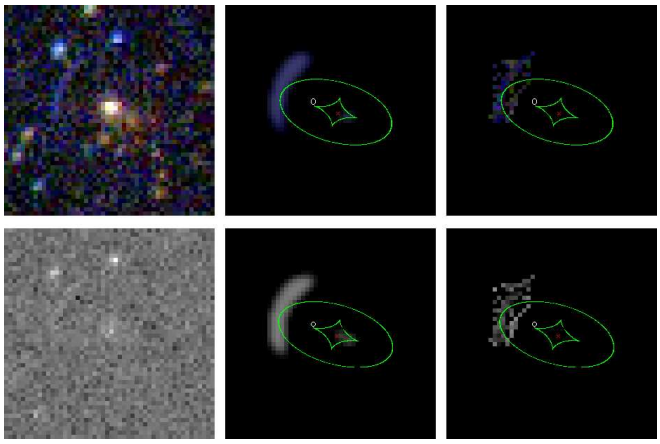

Figure 8. CSWA 8, see Figure 1 for caption.

This lens candidate is a massive galaxy cluster (Ofek et al. 2008). We were able to model this system using a single lens mass component elongated along the axis between the two brightest cluster galaxies, producing a long arc. The counter-image is predicted to lie in the central part of the cluster, in amongst the bright cluster member galaxies: higher resolution, deeper imaging would allow this counter-image to be cleanly separated. Our model has the source being magnified by a factor of 6 ± 2; the lens has Einstein radius 7.8 arcsec.

CSWA 9: SDSS J1227+1725

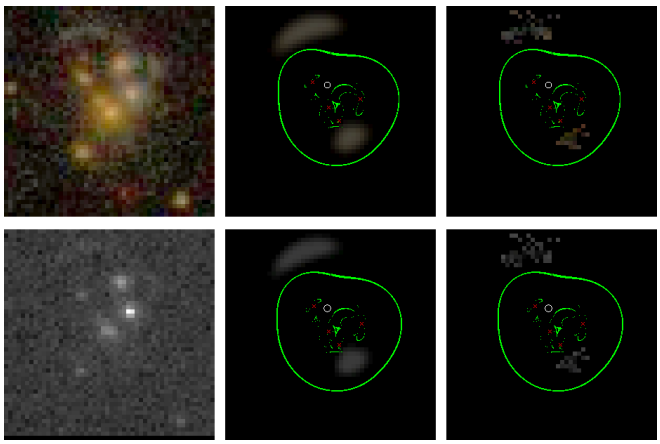

Figure 9. CSWA 9, see Figure 1 for caption.

CSWA 9 is a cluster of galaxies; this lens candidate was modeled using two lens components of comparable mass. Our model successfully reproduces the Northern arc, with a counter-image consistent with the faint emission just South of the BCG. A second, shorter arc to the

North-West, of comparable color to the Northern arc, was not modelled: it may be singly imaged, or have a counter-image buried in the cluster light (if it is indeed a second background source).

CSWA 10: SDSS J2238+1319

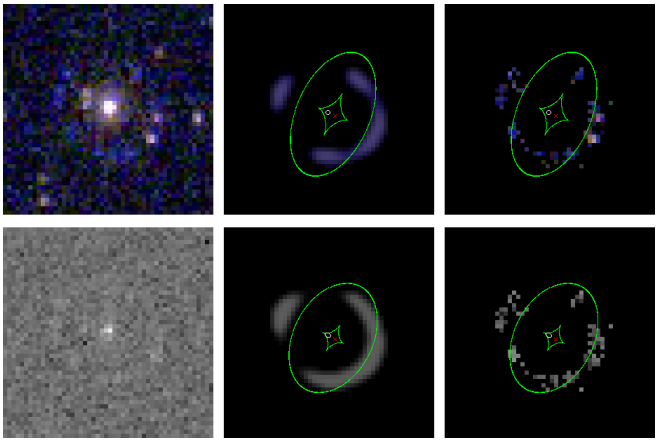

Figure 10. CSWA 10, see Figure 1 for caption.

This candidate is very similar to CSWA 1 in that it consists of three arcs, forming a nearly complete, slightly oval-shaped ring. However, the arcs are observed at quite low signal to noise in the SDSS imaging, and appear broken up as a result. It is also possible that the source is multi-component in nature. We modeled this multiple-imaging system using a single lens and a single source, and were able to reproduce the basic image separation but not the detailed morphology – moreover, two satellite galaxies lie at the arc radius, not detectably perturbing the arc morphology but contributing unlensed brightness to the image. As a result the Ω value for this system is relatively low (42%). The model shown is not unique, in the sense that other combinations of parameters give comparable fits – the Einstein radius of the lens is, however, quite robustly estimated at 9.0 ± 0.1 arcsec.

CSWA 11: SDSS J0800+0812

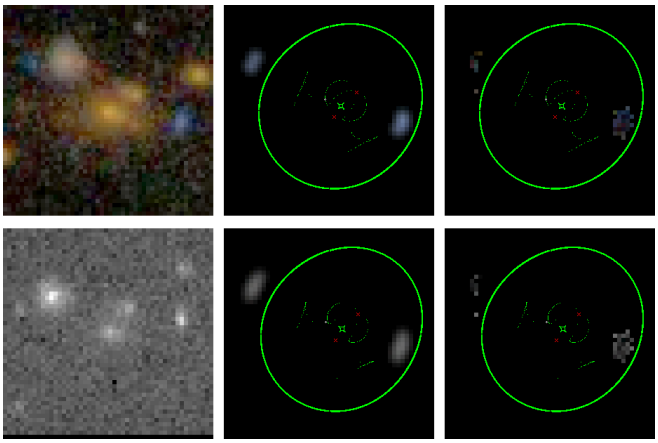

Figure 11. CSWA 11, see Figure 1 for caption.

CSWA 11, like CSWA 10, is a small cluster of galaxies. The candidate arcs are bright blue objects to the East and West of the cluster center. With two lens galaxies and a single source, we were able to reproduce the positions, and relative brightnesses, of the two small blue images quite naturally. However, the predicted arcs were significantly more elongated tangentially than the observed images: this suggests that either the source is smaller than we can model with Mowgli, or we are seeing two unlensed, or weakly lensed, blue objects. The Western blue object may be the bright image of a double, with the counter-image just East of the BCG – such a model would also require a small source to avoid over-predicting the tangential smearing.

The North-Eastern pink-ish object is likely a foreground galaxy which does not contribute as strongly to the lensing taking place. If it were in the same plane as the lensing galaxies, it would tend to cause the North-Eastern image to elongate unless its Einstein radius was under 0.4".

CSWA 12: SDSS J1133+5008

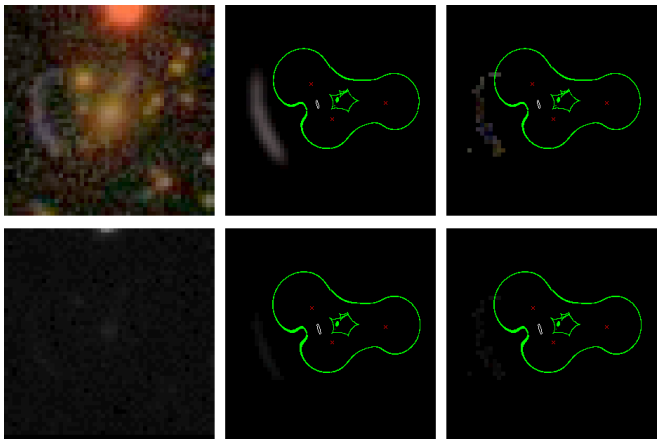

Figure 12. CSWA 12, see Figure 1 for caption.

This small, compact galaxy cluster was modeled using three lens mass components of approximately equal mass, centered on the three most central lens galaxies. This led to some complex caustic structures in the source plane. We were able to produce an arc of approximately the right length and curvature to match the observed feature. Its counter-image is predicted to lie in the central part of the cluster, in amongst the lens galaxies. Its predicted position does not quite match a faint feature of the required matching color, but is close. Note that the counter-images have been masked out in the residual image, an unavoidable consequence of masking the lens galaxies. Overall, the residual image has very few features in it.

CSWA 13: SDSS J1237+5533

This lens candidate, like CSWA 7, can be modeled using a single source and a highly elliptical lens, or using two sources and a lens with lower ellipticity. We show both of these models in Figure 13. As in CSWA 7, the Einstein radius for the two models are very similar.

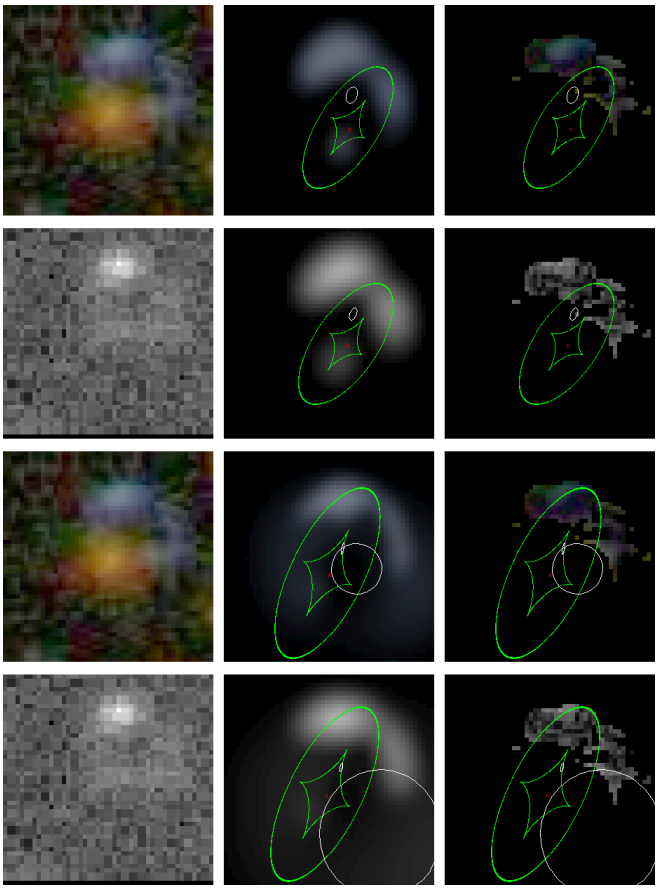

Figure 13. CSWA 13, showing models with one source (top row) and 2 sources (bottom row). Otherwise, see Figure 1 for caption.

This system is so similar to CSWA 7 that much of the same discussion of that object holds here: although the single-source model has a faint residual image, the circular light distribution of the lens does not indicate the highly elliptical lens that is required by this model. However, the dual-source model predicts a prominent counter-image, which does not appear in the astronomical image. The single source model fits the data somewhat better ($\Omega = 86\%$ compared to 71%). Not shown is a third model, with two sources neither of which is multiply-imaged – again, the high brightness of the arcs argues for them being highly magnified, but the evidence for multiple-imaging is not clear-cut.

CSWA 14: SDSS J1723+3411

CSWA 14 is also one of the SDSS bright arc candidates followed up by Kubo et al. (2010), who measured spectroscopic redshifts for both the main lens galaxy and the straight blue arc. This lens candidate is easily modeled using a single source and a single lens. Although our model predicts a counter-image not present in the astronomical image, it is very faint. The predicted arc is also rather more curved than the observed one: it is the high brightness of the blue feature that argues for the source being highly magnified and likely to be strongly lensed. Our model has Einstein radius 3.3 ± 0.1 arcsec, somewhat lower than the rough estimate made by Kubo et al. (2010) of $\simeq 4.7$ arcsec.

CSWA 15: SDSS J1008+1937

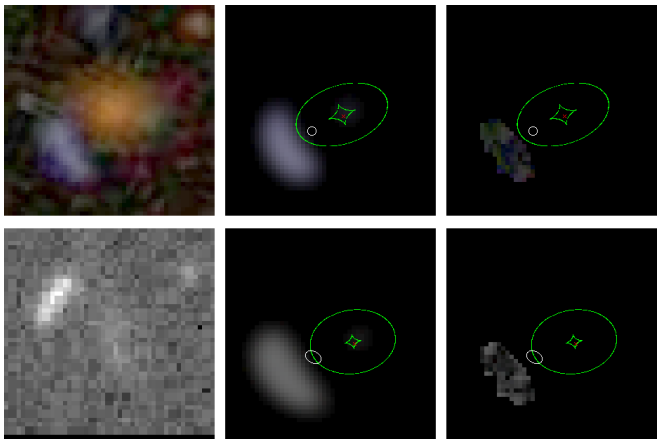

Figure 14. CSWA 14, see Figure 1 for caption.

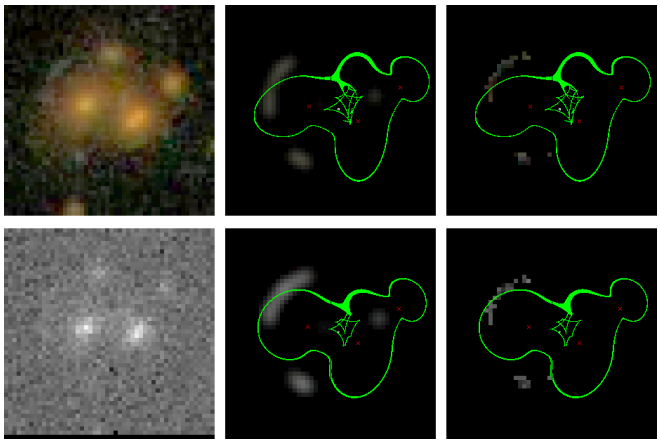

Figure 15. CSWA 15, see Figure 1 for caption.

CSWA 15 is another compact cluster of galaxies, with two central LRGs of comparable brightness, with two satellites to the North and West. The candidate lensed feature is a short, tangentially aligned, curved arc to the North-East of the Eastern main LRG; a small object of comparable colour and surface brighness lies to the South as a candidate counter-image. Modeling the system with three lens components and a single source, we are able to match the positions of the two lensed features, but slightly over predict their elongation. We also predict a faint counter-image (the fourth image of the quad) to the West, where it could lie obscured by the cluster light.

CSWA 16: SDSS J1111+5308

This candidate lens is dominated by a close pair of bright LRGs aligned North-East – South-West, with a further satellite to the South-West. The candidate lensed feature is a pair of blue objects arranged in a curved shape but not aligned tangentially to the LRG pair. It is possible that the green light to the North of the lens is the counter-image to this offset, misaligned arc. Modeling the system with two lens galaxies and a single source, we are only able to reproduce the arc position very roughly: the corresponding predicted counter-image is in approximately the right place, but rather too bright. Adding mass at the position of the satellite galaxy does not improve the model – in fact it makes it harder to predict

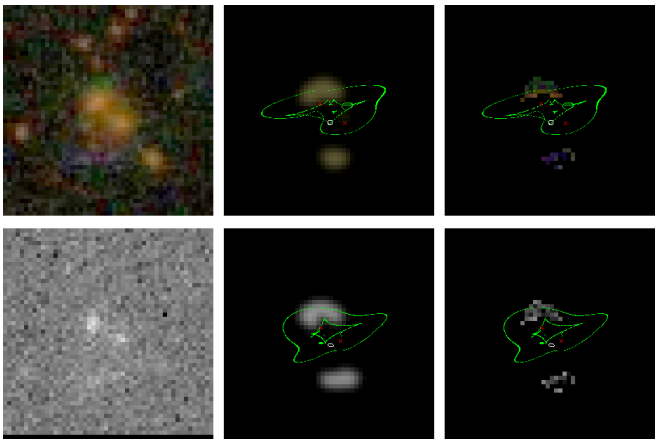

Figure 16. CSWA 16, see Figure 1 for caption.

the candidate arc positions.

CSWA 17: SDSS J1138+2754

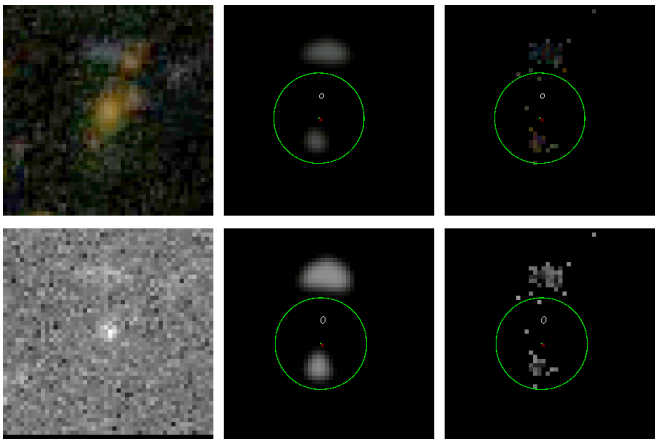

Figure 17. CSWA 17, see Figure 1 for caption.

CSWA 17 is a bright red elliptical galaxy with a short blue arc located just off its major axis; some faint blue emission is just visible on the opposite side of the red galaxy, in the right position for a counter image. This candidate has been modeled using a single lens and a single source. Using a single component lens model, with mass oriented similarly to the lens light, we can predict the arc position and shape reasonably well, with a faint counter-image to the South of the lens galaxy consistent with the faint emission there.

CSWA 18: SDSS J1134+2533

CSWA 18 is the lowest redshift CASSOWARY lens candidate. The candidate lens candidate is part of a linear structure aligned approximately East-West on the sky. The proposed lensed feature is a blue arc spiraling in towards the central LRG. We modelled this candidate using two lens components – the main LRG and a bright satellite to the North-West – and a single source. The arc can be predicted by this model, with the right position, shape and orientation, provided the main lens mass distribution is highly elongated and the source has a low axis ratio (like an edge-on disk). The lens elongation is,

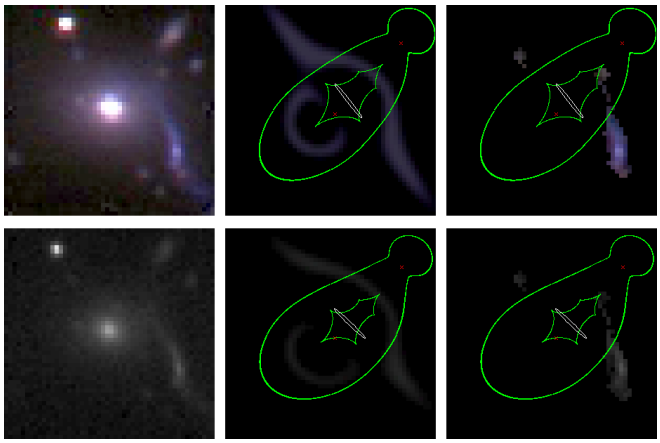

Figure 18. CSWA 18, see Figure 1 for caption.

however, aligned with the larger structure, adding plausibility to this model. The problem is that the model predicts counter arcs of comparable brightness that are not observed: these counter-arcs fall in regions that were masked to remove the lens galaxy light (so that the Ω value is misleadingly high), but they are bright enough to be clearly visible in the original image. Finally, the Einstein radius of the main lens component is some 11 arcsec, very high for such a low redshift, non-cluster lens.

It is very likely that the arc in this image is not a lensed background feature. Instead, the arc might be a one-arm spiral created by a recent interaction. The colors are consistent with the outer disk of the primary galaxy, and the arc seems to be attached to this disk. A measurement of the redshift of the arc would completely resolve this issue. Until then, the difficulty in modeling this system with a plausible mass distribution such that no detectable counter-images are predicted suggests that this is not a typical gravitational lens.

CSWA 19: SDSS J0900+2234

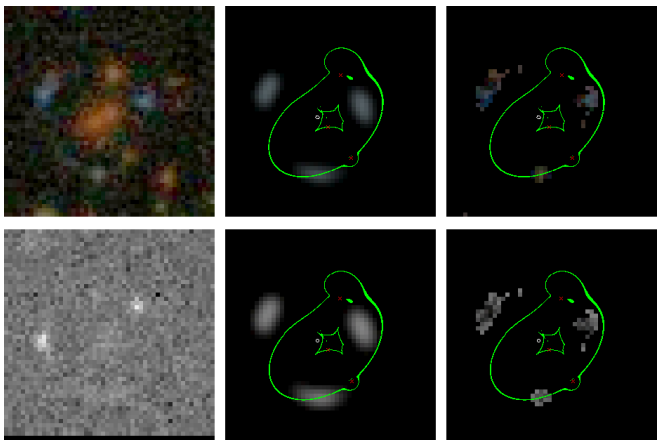

Figure 19. CSWA 19, see Figure 1 for caption.

This candidate was modelled as a simple single-lens system by Diehl et al. (2009), who showed that the blue knots to the West and East of the bright central pair of galaxies have the same redshift. Using a single elliptical mass component centered on and aligned with this pair,

we were able to approximately predict the positions of the two blue images, and predict a counter-arc to the South coincident with third blue-ish image. We obtain a better fit when we include small mass components associated with red satellite galaxies to the North and South: the predicted images also have relative brightnesses that match the observed ones. We note that our predicted image positions are not accurate enough to obtain an Ω better than 44%, and that we can achieve $\Omega \simeq 75\%$ with a model that has three singly-imaged sources. However, the lensing hypothesis has much greater simplicity, and therefore plausibility: with further tweaking we expect the lens model goodness of fit to improve.

The Einstein radius of the main lens component in our model is 6.4 ± 0.1 arcsec, in agreement with the rough estimate of 7 ± 0.8 arcsec from Diehl et al. (2009). Despite the source lying close to a swallowtail caustic the predicted magnification is fairly low (~ 4).

CSWA 20: SDSS J1441+1441

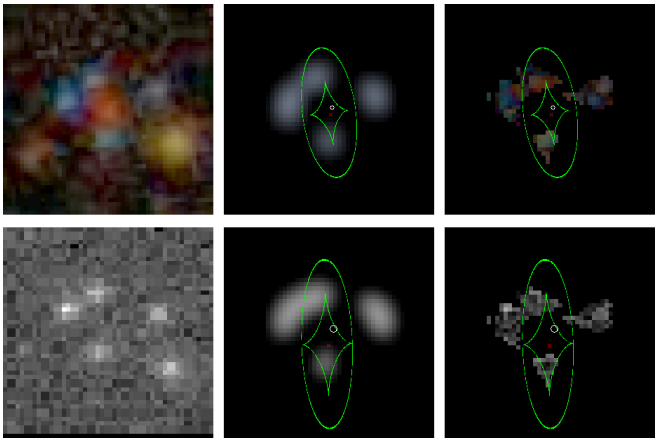

Figure 20. CSWA 20, see Figure 1 for caption.

This candidate is a relatively simple system, a red galaxy apparently lensing a blue source into four images. A model consisting of a single SIE lens and a single source is able to reproduce all four of the image positions accurately.

The Einstein radius of the main lens component is 3.1 ± 0.1 arcsec. Using the redshifts of the source and lens galaxies presented by Pettini et al., we determined the velocity dispersion parameter of the SIE model to be 458 ± 7 km/s, which is within one standard deviation of the stellar velocity dispersion which Pettini et al. (2010) present.

Pettini et al. determined the magnification of this lens to be ~ 6, somewhat lower than that predicted by our model (~ 11).

7.2. *Lens candidate classification*

In the cases where a model's predictions gave a good visual fit to the data, the Ω value was found to be around $80\% - 90\%$. Some models gave lower values – these correspond to mismatches in the detailed morphology of the predicted arcs, and the presence of significant counter-image features. We use these quantified residuals to inform a lens classification.

Based on our modeling, we assign each system a subjective classification, similar to those assigned by *e.g.* Bolton et al. (2008) and Marshall et al. (2009). In this scheme, we use

: "A" to mean "definitely a lens" – a plausible model fits all identified features and does not predict any detectable but unobserved ones.

: "B" to mean "probably a lens" – a plausible model fits most of the identified lensed features, but perhaps not very well in some cases; some models may do better but predict counter-images that may be detectable but are not observed. Likewise, the model may predict the required multiple images very well, but itself be implausible (perhaps containing additional unseen mass components, large centroid offsets, or high ellipticity.

: "C" to mean "possibly a lens" – the features are reminiscent of strong lensing (long, curved arcs or systems of potentially matching conjugate images), but no model can fit them sufficiently well as to provide a convincing multiple imaging scenario. This class includes short, straight, single arcs with no visible counter-images, pairs of images with almost the same color but odd positions and so on.

: "X" to mean "definitely not a lens" – no model can be found which predicts the observed features using multiple imaging.

Typically, good additional data is required to either upgrade a class B candidate to a grade A lens, or to downgrade a C-grade candidate to one in the X class. The CASSOWARY sample is pre-selected to contain candidates that are either grade A, B or C, with a strong preference for A and B grades; we leave the complementary investigation of poorer quality grade C candidates and known (false positive) non-lenses to further work. Our aim here is to show that when the features are due to lensing, we can fit them – and provide a model-based classification (A, B, or C) for all systems in the sample.

7.3. *JPEG and FITS Results*

As mentioned in Section 4.3, the uncertainties of the JPEG and FITS models have been computed independently, in order that they might be compared against each other. Due to JPEG compression, the errors of the JPEG uncertainties tend to be considerably larger than the errors of FITS uncertainties. From the similarity of the inferred parameters in Table ??, we conclude that MOWGLI **may be used to successfully model systems using JPEG images, although the resulting parameter uncertainties will be somewhat less robust.**

We find that the two goodness of fit statistics we use are approximately linearly related to each other, $\hat{\chi}^2_{\rm JPEG} = \gamma \chi^2_{\rm FITS}$. A regression analysis of the 20 analysed systems gives $\gamma = 0.175 \pm 0.70$.

Using linear regression, we determined that $\hat{\chi}^2_{\rm JPEG} \approx 1.34 \chi^2_{\rm FITS} + 106.85$.

Thus, when we chose to let $\delta_{\rm FITS} = 1$ and $\delta_{\rm JPEG} = 1.34$.

ATTENTION PSN! These scalings are inconsistent, which is correct? More seriously, we now have crazy small uncertainties on the parameters, I guess coming from the FITS analysis. I don't believe them! They are obviously too small, no? This could be due to only varying one prameter at a time (the multi-variate likelihood function could be strongly covariant), or there could be a bug. Either way, we cannot publish such values! Fortunately only the table has changed, th e individual notes text is still the same – I'll revisit the referee report and see what we need to do...

7.4. *The Properties of the Sample*

We give the optimized model parameters, and our lens classifications, for the CASSOWARY systems in Table 7.4.

The uncertainties which appear in Table 7.4 were automatically computed by MOWGLI, as described in Section 4.3. The uncertainty of the magnification was found as follows.

Because we found that the magnification uncertainty was dominated by the uncertainty in the PSF and source size, The magnification error due to the uncertainty in the PSF was computed by varying the PSF by $\pm 0.4''$, performing automated parameter optimization for the modified PSF, noting the new magnifications, and comparing the modified magnifications with that of the original model to emulate approximately the full exploration of the PSF width–source size degeneracy.

QUESTION FOR PSN: Did you do this? I only see'X's in the table... Also, 0.4" seems like a lot to get the PSF wrong by - even we are not that innaccurate, are we?!

The magnification errors due to the uncertainty in the source size and position were computed by varying the source size and position (respectively) at fixed PSF width and noting how the magnification responded. The total magnification uncertainty was then estimated by adding in quadrature the uncertainties due to PSF size, source size, and source position These uncertainty values serve to illustrate roughly the available precision when manually modeling imaging data. We note that the derived error bars are not high enough to account for the differences between our magnification estimates and those in the published literature, many of which come from higher quality imaging data.

Following the criteria of the previous subsection, we have confirmed 12 of the 20 candidates in the CASSOWARY sample as class A lensing systems. Of the remaining 8 systems, we classified 6 as class B ("probably a lens"), needing improved data to confirm them as lenses. These include 2 systems, CSWA 7 and CSWA 13, that either need highly elliptical mass distributions inconsistent with their light distributions, or two sources which may not be multiply-imaged. Two systems, CSWA 16 and CSWA 18, we classified as class C or X, since we could not find any good models that explained the position and shape of the proposed arcs and counter-arcs.

We now compare the magnifications and Einstein Radii of the CASSOWARY lenses. For simplicity we make the optimistic assumption that *all* the systems are actually multiple-image systems, and that by fitting the main arcs in each case we have measured accurate Einstein radii. Figure 21 shows the CASSOWARY sample's distribution of apparent Einstein radii: it is shifted to higher values than that of the SLACS and SL2S galaxy-scale lens samples, and is closer to that found in the SL2S group-scale lens search.

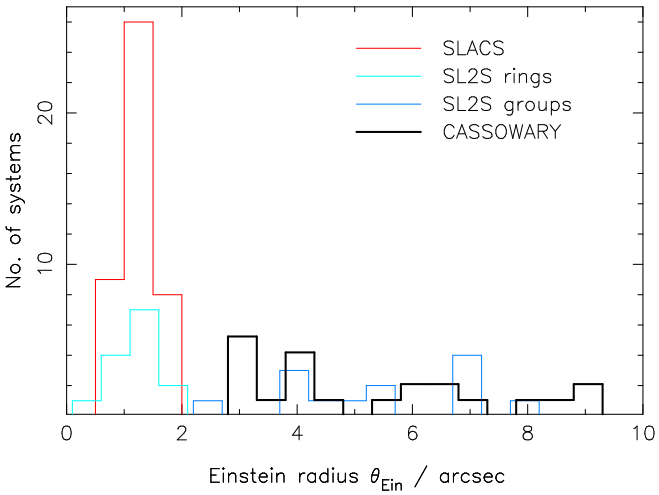

Figure 21. Distribution of apparent Einstein Radii for lenses from the CASSOWARY sample (black), compared with that for the SLACS and SL2S samples. The lowest redshift CASSOWARY candidate, CSWA 18, appears as an outlier: this system is likely not a lens.

Using the lens redshifts in Table 1, we can compute the distance to each CASSOWARY lens and hence the Einstein radius in physical units. In Figure 22 we show the lens redshifts and physical Einstein radii of the CASSOWARY sample, compared with the SL2S and SLACS samples. We see that lenses selected from the SDSS imaging survey tend to be lower redshift (0.3–0.6) than the SL2S group-scale lenses, but have comparable physical Einstein radii (10–50 kpc) – that is, the CASSOWARY systems also have group-scale mass distributions. The lower redshift selection is presumably due to the lower depth of the parent imaging survey (SDSS compared to CFHTLS).

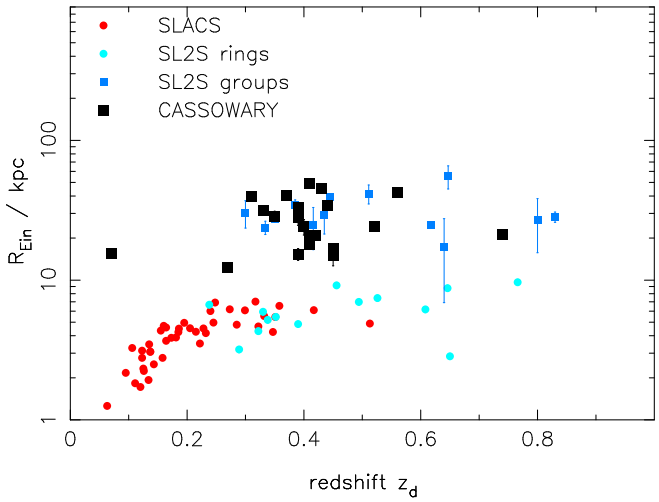

Figure 22. Redshift and physical Einstein radius for the CASSOWARY sample, compared to the SLACS and SL2S lens samples.

Table 2
Parameters for MOWGLI lens models illustrated in Section **??**.

	Lens Properties					Source Prop		
ID	$x_{\rm d}(")$	$y_{\rm d}(")$	$R_{\rm Ein}(")$	$q_{\rm d}$	$\phi_{\rm d}$(rad)	$x_{\rm s}(")$	$y_{\rm s}(")$	$R_{\rm s,eff}$
$1_{\rm F}$	0.0169 ± 0.0003	-0.2958 ± 0.0004	5.7989 ± 0.0002	0.7401 ± 0.0004	0.8023 ± 0.0001	0.2038 ± 0.0002	0.3587 ± 0.0001	$0.3841 \pm$
$1_{\rm J}$	0.1501 ± 0.0001	-0.2783 ± 0.0002	5.9698 ± 0.0003	0.7932 ± 0.0001	0.7698 ± 0.0002	0.2079 ± 0.0001	0.2852 ± 0.0001	$0.3500 \pm$
$2_{\rm F}$	-8.0506 ± 0.0015	-2.0937 ± 0.0025	4.2555 ± 0.0007	0.2310 ± 0.0002	2.1507 ± 0.0003	-1.9886 ± 0.0005	-0.0329 ± 0.0011	$0.6010 \pm$
	0.2207 ± 0.0015	-0.0742 ± 0.0011	6.4141 ± 0.0007	0.7568 ± 0.0003	2.6602 ± 0.0011	-1.9035 ± 0.0009	-1.8186 ± 0.0013	$2.0249 \pm$
$2_{\rm J}$	-8.0125 ± 0.0005	-2.3427 ± 0.0005	6.0308 ± 0.0002	0.9994 ± 0.0002	$0.9592 \pm \infty$	-4.9580 ± 0.0003	1.4778 ± 0.0002	$0.4361 \pm$
	0.9757 ± 0.0003	-1.1786 ± 0.0005	6.0283 ± 0.0002	0.4564 ± 0.0001	0.0072 ± 0.0002	-1.3002 ± 0.0029	-1.9740 ± 0.0023	$1.6940 \pm$
$3_{\rm F}$	1.9394 ± 0.0001	-1.6096 ± 0.0001	3.3300 ± 0.0001	0.3341 ± 0.0001	2.5473 ± 0.0002	0.1051 ± 0.0003	0.1780 ± 0.0001	$0.7824 \pm$
$3_{\rm J}$	1.5830 ± 0.0002	-1.4170 ± 0.0004	3.2320 ± 0.0002	0.3157 ± 0.0001	2.4280 ± 0.0001	0.0829 ± 0.0006	0.0394 ± 0.0002	$0.7387 \pm$
$4_{\rm F}$	$8.2086 \pm \infty$	-0.5885 ± 0.0025	3.7335 ± 0.0018	0.2456 ± 0.0003	0.0811 ± 0.0003	2.3537 ± 0.0015	-1.7409 ± 0.0011	$0.7454 \pm$
	$1.0914 \pm \infty$	-1.8527 ± 0.0051	2.9336 ± 0.0016	0.1651 ± 0.0004	0.7036 ± 0.0009			
	$9.9146 \pm \infty$	-7.2593 ± 0.0045	3.1536 ± 0.0011	0.9615 ± 0.0018	$2.8973 \pm \infty$			
$4_{\rm J}$	8.3751 ± 0.0059	$-0.4255 \pm \infty$	3.6577 ± 0.0008	0.1953 ± 0.0002	0.0873 ± 0.0003	2.0995 ± 0.0011	-1.8531 ± 0.0011	$0.8645 \pm$
	1.2606 ± 0.0012	-1.9388 ± 0.0052	3.0402 ± 0.0014	0.1787 ± 0.0003	0.6396 ± 0.0008			
	$10.0072 \pm \infty$	-7.4411 ± 0.0038	3.4522 ± 0.0006	0.9748 ± 0.0012	$2.7109 \pm \infty$			
$5_{\rm F}$	2.7521 ± 0.0002	0.7986 ± 0.0002	1.6331 ± 0.0001	1.0000 ± 0.0002	$2.1262 \pm \infty$	-0.8848 ± 0.0001	-0.2669 ± 0.0001	$0.1683 \pm$
	-2.9701 ± 0.0001	-0.3090 ± 0.0001	2.2273 ± 0.0001	1.0000 ± 0.0001	$2.2294 \pm \infty$			
$5_{\rm J}$	3.0801 ± 0.0006	0.5010 ± 0.0003	1.7504 ± 0.0001	1.0000 ± 0.0002	$1.7308 \pm \infty$	-0.6741 ± 0.0001	-0.5202 ± 0.0001	$0.2710 \pm$
	-3.0522 ± 0.0002	-0.4250 ± 0.0001	2.1884 ± 0.0002	1.0000 ± 0.0001	$2.1291 \pm \infty$			
$6_{\rm F}$	-0.4670 ± 0.0005	-0.4550 ± 0.0005	3.8912 ± 0.0006	0.5697 ± 0.0004	0.2607 ± 0.0002	0.7791 ± 0.0003	0.4362 ± 0.0005	$0.3499 \pm$
$6_{\rm J}$	-0.0057 ± 0.0005	-0.4325 ± 0.0004	3.7760 ± 0.0003	0.6094 ± 0.0002	0.2377 ± 0.0002	0.8456 ± 0.0002	0.1351 ± 0.0001	$0.2926 \pm$
$7a_{\rm F}$	-0.6025 ± 0.0005	-0.0228 ± 0.0002	2.4870 ± 0.0002	0.1794 ± 0.0001	2.6766 ± 0.0001	-2.0853 ± 0.0001	0.9694 ± 0.0001	$0.1545 \pm$
$7a_{\rm J}$	-0.3032 ± 0.0003	-0.1576 ± 0.0002	2.6177 ± 0.0002	0.1888 ± 0.0001	2.7032 ± 0.0002	-1.7920 ± 0.0002	0.7744 ± 0.0001	$0.2925 \pm$
$7b_{\rm F}$	0.3338 ± 0.0005	-0.4025 ± 0.0002	2.7504 ± 0.0001	0.6659 ± 0.0001	2.8370 ± 0.0003	-1.0126 ± 0.0002	1.0919 ± 0.0005	$0.1071 \pm$
						-1.3525 ± 0.0002	-0.0321 ± 0.0002	$0.1659 \pm$
$7b_{\rm J}$	0.4957 ± 0.0002	-0.5641 ± 0.0002	2.7608 ± 0.0004	0.7092 ± 0.0001	2.7348 ± 0.0003	-0.7565 ± 0.0009	0.9445 ± 0.0005	$0.1672 \pm$
						-1.2015 ± 0.0002	-0.1493 ± 0.0002	$0.3554 \pm$
$8_{\rm F}$	0.9384 ± 0.0067	-0.1077 ± 0.0046	7.8527 ± 0.0012	0.5007 ± 0.0008	2.8410 ± 0.0016	-3.2155 ± 0.0033	1.8441 ± 0.0046	$0.4260 \pm$
$8_{\rm J}$	0.6438 ± 0.0004	-0.0912 ± 0.0006	7.8033 ± 0.0003	0.4324 ± 0.0001	2.8342 ± 0.0002	-3.4690 ± 0.0004	1.7599 ± 0.0002	$0.2748 \pm$
$9_{\rm F}$	$4.1022 \pm \infty$	$1.8575 \pm \infty$	2.2421 ± 0.0035	0.9288 ± 0.0041	$0.6904 \pm \infty$	-0.4267 ± 0.0028	3.7810 ± 0.0053	$0.4968 \pm$
	-0.5513 ± 0.0093	$0.8088 \pm \infty$	2.4443 ± 0.0032	$0.9641 \pm \infty$	$0.9707 \pm \infty$			
	$0.8718 \pm \infty$	$-1.0032 \pm \infty$	2.9535 ± 0.0030	1.0000 ± 0.0028	$1.3654 \pm \infty$			
	$-2.6316 \pm \infty$	$4.3168 \pm \infty$	1.1984 ± 0.0036	1.0000 ± 0.0077	$1.7704 \pm \infty$			
$9_{\rm J}$	3.9018 ± 0.0028	$2.1214 \pm \infty$	2.2290 ± 0.0010	0.9542 ± 0.0010	$0.8754 \pm \infty$	-0.4526 ± 0.0008	3.7158 ± 0.0014	$0.4098 \pm$
	-0.6751 ± 0.0044	0.8817 ± 0.0050	2.3430 ± 0.0010	0.9205 ± 0.0014	$1.1304 \pm \infty$			
	0.7991 ± 0.0036	-0.9545 ± 0.0024	2.9005 ± 0.0010	1.0000 ± 0.0015	$1.4358 \pm \infty$			
	$-2.8187 \pm \infty$	$4.4102 \pm \infty$	1.2373 ± 0.0006	0.9724 ± 0.0023	$1.7748 \pm \infty$			
$10_{\rm F}$	0.7027 ± 0.0051	-0.9249 ± 0.0019	9.0240 ± 0.0011	0.6828 ± 0.0007	1.0731 ± 0.0005	-0.2558 ± 0.0016	-0.4439 ± 0.0010	$0.5349 \pm$
$10_{\rm J}$	0.7583 ± 0.0002	-0.8487 ± 0.0001	9.1335 ± 0.0001	0.5905 ± 0.0001	1.1570 ± 0.0001	-0.0699 ± 0.0004	-0.4907 ± 0.0001	$0.4208 \pm$

Notes: The subscripts "F" and "J" denote parameters inferred given data in FITS and JPEG formats respectively.

Figure 23 shows the distribution of lens magnifications across the sample; these appear similar to the SLACS systems. However, we saw from comparing our MOWGLI models with those in the literature based on improved data (in Section 7.1) that in many (but perhaps not all) cases the MOWGLI models may be underestimating the total magnification: the systematic offset noted in the better measured CASSOWARY systems is typically in the direction of smaller magnifications. This suggests that were this to be corrected for, the CASSOWARY systems could actually have higher magnification than the SLACS lenses. One explanation for this could be that group-scale lenses have caustics of larger angular size, as seen in Figure 21, such that distant galaxies of subarcsecond size can sample the high magnification parts of the source plane better. Sources that are large compared to the high magnification regions tend to blur this out, leading to lower total magnification. However, more accurate models will be needed to test this.

8. DISCUSSION

We have demonstrated MOWGLI's effectiveness by modeling the twenty candidate lens systems from the CASSOWARY sample. Within the near future, we plan to integrate this tool into a citizen science portal like

Table 2
Parameters for Mowgli lens models (continued).

	Lens Properties					Source Pr		
ID	$x_{\rm d}$(")	$y_{\rm d}$(")	$R_{\rm Ein}$(")	$q_{\rm d}$	$\phi_{\rm d}$(rad)	$x_{\rm s}$(")	$y_{\rm s}$(")	$R_{\rm s,}$
$11_{\rm F}$	$3.8732 \pm \infty$	3.0742 ± 0.0034	4.2789 ± 0.0027	1.0000 ± 0.0007	$1.7169 \pm \infty$	-0.4356 ± 0.0016	1.6677 ± 0.0023	0.1115
	$0.6263 \pm \infty$	-0.6679 ± 0.0037	7.3386 ± 0.0019	1.0000 ± 0.0005	$2.6255 \pm \infty$			
$11_{\rm J}$	3.6825 ± 0.0011	2.8283 ± 0.0007	4.4517 ± 0.0002	1.0000 ± 0.0003	$1.8910 \pm \infty$	-0.5172 ± 0.0002	1.5690 ± 0.0002	0.0652
	0.4424 ± 0.0011	-0.6674 ± 0.0008	7.2584 ± 0.0002	1.0000 ± 0.0001	$2.6149 \pm \infty$			
$12_{\rm F}$	$7.6663 \pm \infty$	$1.1792 \pm \infty$	3.3069 ± 0.0016	1.0000 ± 0.0013	$0.0052 \pm \infty$	-1.4875 ± 0.0016	0.5317 ± 0.0067	0.855
	$-2.9888 \pm \infty$	$4.0137 \pm \infty$	3.0207 ± 0.0019	0.9318 ± 0.0060	$1.1288 \pm \infty$			
	$-0.0149 \pm \infty$	$-0.9929 \pm \infty$	2.5277 ± 0.0016	1.0000 ± 0.0015	$0.1665 \pm \infty$			
$12_{\rm J}$	$7.6139 \pm \infty$	$1.2778 \pm \infty$	3.1730 ± 0.0008	1.0000 ± 0.0018	$0.0770 \pm \infty$	-1.8455 ± 0.0007	0.8473 ± 0.0022	0.6046
	$-3.0211 \pm \infty$	4.0744 ± 0.0062	2.9858 ± 0.0010	0.9605 ± 0.0052	$1.1571 \pm \infty$			
	$-0.0736 \pm \infty$	$-0.9905 \pm \infty$	2.5128 ± 0.0010	0.9893 ± 0.0015	$0.1648 \pm \infty$			
$13a_{\rm F}$	1.1687 ± 0.0001	-0.5498 ± 0.0001	3.2730 ± 0.0003	0.4396 ± 0.0002	0.9202 ± 0.0001	1.7180 ± 0.0001	1.3934 ± 0.0001	0.3930
$13a_{\rm J}$	1.0681 ± 0.0002	-1.1484 ± 0.0001	3.2159 ± 0.0002	0.3700 ± 0.0001	0.8299 ± 0.0001	1.7529 ± 0.0001	1.1180 ± 0.0001	0.5160
$13b_{\rm F}$	-0.3071 ± 0.0003	-0.9856 ± 0.0002	4.1735 ± 0.0004	0.3922 ± 0.0001	1.1025 ± 0.0001	$6.3856 \pm \infty$	$-7.6777 \pm \infty$	7.901
						0.9320 ± 0.0003	0.8400 ± 0.0003	0.3348
$13b_{\rm J}$	-0.1455 ± 0.0001	-1.1560 ± 0.0001	4.1152 ± 0.0001	0.3918 ± 0.0001	1.1161 ± 0.0001	$1.7884 \pm \infty$	$-0.1387 \pm \infty$	3.5318
						0.9848 ± 0.0001	0.5818 ± 0.0001	0.4257
$14_{\rm F}$	0.2855 ± 0.0005	0.5375 ± 0.0007	2.2143 ± 0.0007	0.6570 ± 0.0011	0.4914 ± 0.0004	-1.6613 ± 0.0005	-1.5908 ± 0.0002	0.3685
$14_{\rm J}$	1.2830 ± 0.0006	-0.4478 ± 0.0002	2.6560 ± 0.0003	0.8593 ± 0.0007	0.1449 ± 0.0011	-0.9460 ± 0.0003	-1.5324 ± 0.0006	0.4111
$15_{\rm F}$	3.6384 ± 0.0016	-1.0963 ± 0.0015	4.2547 ± 0.0004	0.6193 ± 0.0002	1.4837 ± 0.0006	1.0928 ± 0.0004	0.3108 ± 0.0005	0.0854
	-3.6035 ± 0.0012	1.2487 ± 0.0012	4.0922 ± 0.0003	0.7864 ± 0.0008	0.1741 ± 0.0003			
	9.4912 ± 0.0048	$3.8869 \pm \infty$	1.7615 ± 0.0004	0.9923 ± 0.0016	$1.5221 \pm \infty$			
$15_{\rm J}$	3.6585 ± 0.0013	-1.2222 ± 0.0008	4.2031 ± 0.0007	0.4694 ± 0.0001	1.5588 ± 0.0006	1.1736 ± 0.0008	0.2526 ± 0.0004	0.1219
	-3.3942 ± 0.0018	0.9264 ± 0.0018	4.0326 ± 0.0007	0.5514 ± 0.0003	0.3005 ± 0.0009			
	9.6965 ± 0.0049	3.5152 ± 0.0011	1.9235 ± 0.0005	1.0000 ± 0.0010	$1.4582 \pm \infty$			
$16_{\rm F}$	-1.2966 ± 0.0028	1.1609 ± 0.0019	3.0630 ± 0.0022	0.4625 ± 0.0008	0.1007 ± 0.0019	0.1364 ± 0.0024	-1.6100 ± 0.0014	0.4591
	1.3258 ± 0.0079	$-1.0575 \pm \infty$	2.0227 ± 0.0014	0.4161 ± 0.0072	$0.4015 \pm \infty$			
$16_{\rm J}$	-1.2927 ± 0.0013	1.1632 ± 0.0002	3.0009 ± 0.0004	0.2450 ± 0.0001	0.0986 ± 0.0002	-0.0720 ± 0.0005	-1.7158 ± 0.0002	0.2929
	2.0187 ± 0.0016	-1.1437 ± 0.0034	1.8085 ± 0.0002	0.2246 ± 0.0002	0.4238 ± 0.0005			
$17_{\rm F}$	-1.206 ± 0.650	-1.372 ± 5.350	6.469 ± 0.950	1.000 ± 0.400	$0.027 \pm \infty$	-0.890 ± 0.550	1.984 ± 0.850	0.486
$17_{\rm J}$	-1.3885 ± 0.0009	-1.1222 ± 0.0016	6.3222 ± 0.0004	0.9629 ± 0.0005	0.2039 ± 0.0047	-0.9775 ± 0.0007	2.0026 ± 0.0011	0.5101
$18_{\rm F}$	0.5032 ± 0.0000	-0.4251 ± 0.0000	11.2594 ± 0.0000	0.6394 ± 0.0000	0.5737 ± 0.0000	3.6841 ± 0.0000	1.9537 ± 0.0000	4.0563
	13.1564 ± 0.0000	13.0103 ± 0.0000	2.8434 ± 0.0000	0.9983 ± 0.0000	0.1873 ± 0.0000			
$18_{\rm J}$	0.7022 ± 0.0001	-0.4503 ± 0.0001	11.1873 ± 0.0001	0.5119 ± 0.0001	0.7645 ± 0.0001	2.8205 ± 0.0001	2.4927 ± 0.0001	1.0605
	13.0795 ± 0.0002	13.0800 ± 0.0027	2.8933 ± 0.0001	1.0000 ± 0.0003	$0.1672 \pm \infty$			
$19_{\rm F}$	1.0621 ± 0.0020	5.5164 ± 0.0041	1.3539 ± 0.0046	0.8442 ± 0.0020	1.7365 ± 0.0027	$13.7923 \pm \infty$	$-27.3317 \pm \infty$	3.127
	$2.7154 \pm \infty$	$-6.3600 \pm \infty$	0.2274 ± 0.0012	$0.9604 \pm \infty$	$1.3984 \pm \infty$	-1.8373 ± 0.0003	-0.8960 ± 0.0023	0.2472
	-0.5262 ± 0.0011	$-1.9317 \pm \infty$	6.5892 ± 0.0004	0.6063 ± 0.0002	0.6555 ± 0.0004			
$19_{\rm J}$	1.1148 ± 0.0015	5.4609 ± 0.0012	1.3834 ± 0.0002	0.8429 ± 0.0005	1.7136 ± 0.0012	$13.5063 \pm \infty$	$-25.5931 \pm \infty$	0.855
	$2.6969 \pm \infty$	$-6.3533 \pm \infty$	0.2046 ± 0.0002	0.8476 ± 0.0028	$1.4884 \pm \infty$	-1.8750 ± 0.0002	-0.8329 ± 0.0003	0.2658
	-0.6527 ± 0.0002	-1.9377 ± 0.0011	6.6062 ± 0.0002	0.6238 ± 0.0001	0.6471 ± 0.0002			
$20_{\rm F}$	-0.1721 ± 0.0001	-0.7929 ± 0.0001	3.3043 ± 0.0005	0.2965 ± 0.0002	1.6060 ± 0.0002	0.2704 ± 0.0001	0.2919 ± 0.0001	0.2298
$20_{\rm J}$	-0.0505 ± 0.0002	-0.1944 ± 0.0003	2.9641 ± 0.0002	0.3978 ± 0.0001	1.7197 ± 0.0002	0.2126 ± 0.0001	0.1580 ± 0.0001	0.1293

Notes: The subscripts "F" and "J" denote parameters inferred given data in FITS and JPEG formats respectively.

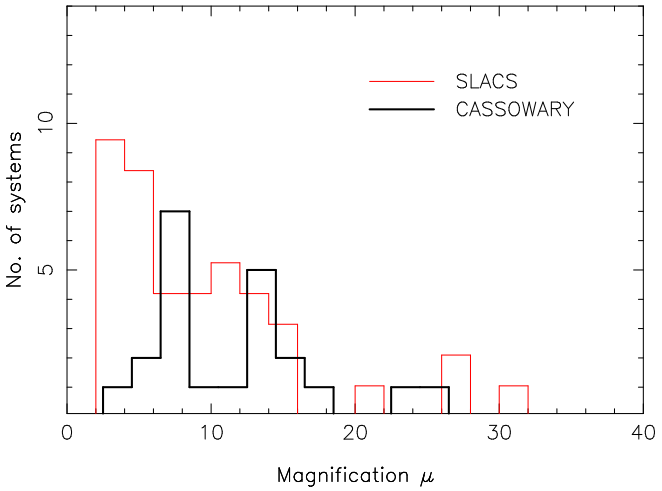

Figure 23. Distribution of magnifications for lenses from the CASSOWARY sample (black), compared with the that for the SLACS sample (red). As seen in Section 7.1, MOWGLI tends to underestimate magnification, such that the values plotted here may be lower limits. This suggests that the CASSOWARY lenses may be systematically higher magnification than the SLACS lenses.

Galaxy Zoo to enable distributed gravitational lens identification analysis. The goal is to turn candidates into discoveries through model-based classification, with the work done by a subset of Zoo users who are motivated by analysing astronomical data in more detail.

Once users are familiarized with gravitational lensing and modeling, they will be able to generate models fairly rapidly. We presented MOWGLI to a high school student: after completing a short tutorial on gravitational lensing and becoming familiarized with the MOWGLI interface, he was able to achieve crude models within ten minutes per candidate. After spending another forty-five to sixty minutes on each model, he was able to produce results comparable to those presented in this paper. Those with backgrounds in gravitational lensing are able to produce models in significantly less time. The authors of this paper are able to produce reasonably accurate models in as little as three minutes, although refining the models to optimise the goodness of fit can take considerably longer. We note that the modeling time *includes* the masking of the lens galaxies. We can compare this to a range of automated routine operation times. The HAGGLeS robot requires about 30 seconds per candidate, to do both lens light subtraction and lensed feature modeling. As referred to above, this procedure is currently restricted to very simple single-component lens models, and a significant fraction of the results need further inspection if the search is to be highly complete. At the other end of the scale, robust MCMC searches of model parameter space have been carried out for known lenses (Marshall et al. 2007; Jullo et al. 2007; Vegetti & Koopmans 2009, *e.g.*), but these analyses typically take between hours and days of computation time.

While manual modeling seems to be an effective way of quickly understanding complex lens candidates, as computing speed continues to increase we can consider a automated procedures that somehow manage to do a rigorous parameter space exploration in a usefully short time. A first step towards this could be to enable MOWGLI to automatically explore the parameter space about the points in parameter space that the user believes to fit the data well. The human-generated models will certainly be useful in finding the starting points for these more finely tuned automated models. Another important way the human user contributes is by intelligently masking the data. Confusion with non-lensed image features is perhaps the biggest obstacle for an automated lens finder, while humans can very efficiently spot features they think might be lensed. Indeed, we might consider asking citizens to identify arcs manually (perhaps with a painting tool) rather than blocking out non-arcs.

One technical improvement worth consideration is automatic flexible source model optimisation, as performed on pixel grids by, e.g. ? and ?. This would remove the need to place a source in amongst the caustics, but rather simply transform the observed images to the source plane: the constraints on the model then come from the regularization of the source, with models that preserve as much dark sky as possible favored. This may well make lens modeling more intuitive, and make the parameter space exploration easier. We will investigate this in a future paper.

Another way to increase the accuracy of the modeling would be to provide a PSF image directly, perhaps one derived from nearby field stars. However, in future we expect model PSFs to be provided with all requested cutout survey images. The current SDSS images have a simple double Gaussian PSF model provided with them, but in future this is likely the become more sophisticated as the image quality improves. In any case, we find that the PSF model is only an important source of uncertainty for certain parameters (such as source magnitude and total magnification): the astrometry is largely insensitive to the exact model PSF assumed.

While we have shown MOWGLI to be a useful tool for modeling systems within the CASSOWARY sample, certain technical modifications suggest themselves. Some of the systems in the sample have multiple lens and source planes. It is not yet clear whether multiple lens planes are *required* for lens identification: CSWA 2 is interesting in this regard. Other complications that may need to be taken into account include varying the PSF width at the same time as the lens and source model (if the PSF is not well known); this facility would perhaps have made some of the magnification estimates in this paper more accurate. In terms of ease of use, we may need to allow the user to begin with simple modeling, and only later add more complexity to the model as a solution is converged upon.

While we have succeeded at quantifying the goodness of fit of a model, our method fails to penalize bad models where extraneous predicted arcs which appear in masked regions. These hidden arcs do not affect the goodness of fit, which allows models which clearly do not fit the data to achieve high Ω values. This is further motivation for first generating images of lensed features – the blank parts of this image can be used to reject models that predict features there.

We identified an important systematic error by comparing the total magnifications provided by the MOWGLI models with corresponding values in the literature: the disagreement is in most cases larger than our estimates

of the magnification uncertainty. Magnification is quite sensitive to source compactness as well as size (see *e.g.* Orban de Xivry & Marshall 2009) – our assumption of a Gaussian profile source is one possible source of error. Another cause could be insufficient resolution in the deflection angle grids that we use: sub-sampling, or even adaptive gridding, should give more accurate results, at the cost of some computation speed. Likewise, larger, sub-sampled PSF model grids would provide more slower but more accurate image predictions.

Because of the ease with which models may be obtained using MOWGLI, it ought to be a useful tool which will enable citizen scientists to contribute to analyzing and modeling candidates from large-scale surveys. Nevertheless, citizen scientists must be familiarized with gravitational lensing and modeling in order to effectively use this applet. For this reason, it will be necessary to design carefully a help system – perhaps including an interactive tutorial for citizen scientists to complete before making positive contributions to the modeling of candidate lens systems.

In the near term, while its development continues and it begins to be used by citizens for lens detection, MOWGLI has an obvious application in education. It could be used as a teaching aid in undergraduate labs to help students gain intuition on the morphology of gravitational lensing systems, and learn about modeling data and how to quantify goodness of fit. It will also be helpful in training research students who are starting to work with gravitational lenses.

9. CONCLUSIONS

MOWGLI is a tool for manually modeling gravitational lensing systems, that can be used by students, researchers, and citizen scientists alike. We have demonstrated the usefulness of MOWGLI by fitting models to the CASSOWARY sample of SDSS lens candidates. We draw the following conclusions:

- A manual model of a typical lensing system can be constructed in a few minutes by an expert user, and only a factor of ten longer by a novice. This is longer than simple automated search robots take to classify simple lenses, but considerably less than robust searches of complex lens model parameter space.
- We have confirmed 12 of the twenty candidates within the CASSOWARY sample to be lensing systems. Six of the remainder are at least likely to be causing high magnification of a background object, and evidence of multiple imaging may come to light with improved data. We were unable to find satisfactory lens models for two of the candidates.
- The CASSOWARY lenses have comparable Einstein radii to the group-scale lenses found in the SL2S survey, but are at somewhat lower redshift. More detailed comparisons between these two samples may provide useful insights into the evolution of massive galaxies and groups since redshift 0.5.

Detailed studies of the thousands of complex lens systems identified in upcoming large surveys will provide powerful constraints on models of galaxy structure and evolution, and will result in giant arrays of well-calibrated cosmic telescopes. Enabling citizens to participate in this enterprise is not only a very exciting education and outreach opportunity; they can play an important role in generating a large sample of manually-modeled lens candidates, from which more accurate models can be made and more effective automated algorithms developed.

MOWGLI is available for all to use at `http://ephysics.org/mowgli`.

We thank Layne Wright, of the Galaxy Zoo lens forum, for detailed comments on the operation of MOWGLI, and Brad Strylowski for evaluating MOWGLI as a high schooler. We are grateful to Aprajita Verma, Arfon Smith, Michael Parrish and Chris Lintott for providing feedback from the Galaxy Zoo perspective, and to Eli Rykoff for useful discussions on aspects of intuitiveness in gravitational lens simulation during the development of the iPhone application "gravlens." We thank the anonymous referee for valuable suggestions leading to a more comprehensive study. The work of JFW and PSN was supported by the National Science Foundation under Grants No. DMS-0639300 and AST-0941610. The work of PJM was supported in part by the U.S. Department of Energy under contract number DE-AC02-76SF00515, and by the Kavli Foundation and the Royal Society in the form of research fellowships. This material is based upon work supported by the National Science Foundation under Grants No. DMS-0639300 and AST-0941610.

REFERENCES

Abazajian, K. N., et al. 2009, ApJS, 182, 543
Allam, S. S., Tucker, D. L., Lin, H., Diehl, H. T., Annis, J., Buckley-Geer, E. J., & Frieman, J. A. 2007, ApJ, 662, L51
Auger, M. W., Treu, T., Bolton, A. S., Gavazzi, R., Koopmans, L. V. E., Marshall, P. J., Bundy, K., & Moustakas, L. A. 2009, ApJ, 705, 1099
Belokurov, V., Evans, N. W., Hewett, P. C., Moiseev, A., McMahon, R. G., Sanchez, S. F., & King, L. J. 2009, MNRAS, 392, 104
Belokurov, V., Evans, N. W., Moiseev, A., King, L. J., Hewett, P. C., Pettini, M., Wyrzykowski, L., McMahon, R. G., Smith, M. C., Gilmore, G., Sanchez, S. F., Udalski, A., Koposov, S., Zucker, D. B., & Walcher, C. J. 2007, ApJ, 671, L9
Benítez, N., Ford, H., Bouwens, R., Menanteau, F., Blakeslee, J., Gronwall, C., Illingworth, G., Meurer, G., Broadhurst, T. J., Clampin, M., Franx, M., Hartig, G. F., Magee, D., Sirianni, M., Ardila, D. R., Bartko, F., Brown, R. A., Burrows, C. J., Cheng, E. S., Cross, N. J. G., Feldman, P. D., Golimowski, D. A., Infante, L., Kimble, R. A., Krist, J. E., Lesser, M. P., Levay, Z., Martel, A. R., Miley, G. K., Postman, M., Rosati, P., Sparks, W. B., Tran, H. D., Tsvetanov, Z. I., White, R. L., & Zheng, W. 2004, ApJS, 150, 1
Blain, A. W., Kneib, J., Ivison, R. J., & Smail, I. 1999, ApJ, 512, L87
Bolton, A. S., Burles, S., Koopmans, L. V. E., Treu, T., Gavazzi, R., Moustakas, L. A., Wayth, R., & Schlegel, D. J. 2008, ApJ, 682, 964
Bolton, A. S., Burles, S., Koopmans, L. V. E., Treu, T., & Moustakas, L. A. 2006, ApJ, 638, 703
Bradač, M., Clowe, D., Gonzalez, A. H., Marshall, P., Forman, W., Jones, C., Markevitch, M., Randall, S., Schrabback, T., & Zaritsky, D. 2006, ApJ, 652, 937
Bradač, M., Treu, T., Applegate, D., Gonzalez, A. H., Clowe, D., Forman, W., Jones, C., Marshall, P., Schneider, P., & Zaritsky, D. 2009, ApJ, 706, 1201
Brewer, B. J., Lewis, G. F., Belokurov, V., Irwin, M. J., Bridges, T. J., & Wyn Evans, N. 2010, ArXiv e-prints
Browne, I. W. A., et al. 2003, MNRAS, 341, 13

Cabanac, R. A., Alard, C., Dantel-Fort, M., Fort, B., Gavazzi, R., Gomez, P., Kneib, J. P., Le Fèvre, O., Mellier, Y., Pello, R., Soucail, G., Sygnet, J. F., & Valls-Gabaud, D. 2007, A&A, 461, 813
Cardamone, C., Schawinski, K., Sarzi, M., Bamford, S. P., Bennert, N., Urry, C. M., Lintott, C., Keel, W. C., Parejko, J., Nichol, R. C., Thomas, D., Andreescu, D., Murray, P., Raddick, M. J., Slosar, A., Szalay, A., & Vandenberg, J. 2009, MNRAS, 399, 1191
Christensen, L., D'Odorico, S., Pettini, M., Belokurov, V., Evans, N. W., Kellogg, M., & Vernet, J. 2010, MNRAS, 804
Diehl, H. T., Allam, S. S., Annis, J., Buckley-Geer, E. J., Frieman, J. A., Kubik, D., Kubo, J. M., Lin, H., Tucker, D., & West, A. 2009, ApJ, 707, 686
Dye, S., Evans, N. W., Belokurov, V., Warren, S. J., & Hewett, P. 2008, MNRAS, 388, 384
Faure, C., et al. 2008, ApJS, 176, 19
Fort, B. 1987, S&T, 74, 581
Gavazzi, R., Treu, T., Rhodes, J. D., Koopmans, L. V., Bolton, A. S., Burles, S., Massey, R., & Moustakas, L. A. 2007, ArXiv Astrophysics e-prints
Hennawi, J. F., Gladders, M. D., Oguri, M., Dalal, N., Koester, B., Natarajan, P., Strauss, M. A., Inada, N., Kayo, I., Lin, H., Lampeitl, H., Annis, J., Bahcall, N. A., & Schneider, D. P. 2008, AJ, 135, 664
Holincheck, A., Wallin, J., Borne, K., Lintott, C., Smith, A., Bamford, S., & Fortson, L. 2010, in Astronomical Society of the Pacific Conference Series, Vol. 423, Astronomical Society of the Pacific Conference Series, ed. B. Smith, J. Higdon, S. Higdon, & N. Bastian, 223
Jackson, N. 2008, MNRAS, 389, 1311
Jullo, E., Kneib, J., Limousin, M., Elíasdóttir, Á., Marshall, P. J., & Verdugo, T. 2007, New Journal of Physics, 9, 447
Kneib, J. P., Mellier, Y., Fort, B., & Mathez, G. 1993, A&A, 273, 367
Koopmans, L. V. E., Bolton, A., Treu, T., Czoske, O., Auger, M. W., Barnabè, M., Vegetti, S., Gavazzi, R., Moustakas, L. A., & Burles, S. 2009, ApJ, 703, L51
Koopmans, L. V. E., Treu, T., Fassnacht, C. D., Blandford, R. D., & Surpi, G. 2003, ApJ, 599, 70
Kormann, R., Schneider, P., & Bartelmann, M. 1994, A&A, 284, 285
Kubo, J. M., Allam, S. S., Annis, J., Buckley-Geer, E. J., Diehl, H. T., Kubik, D., Lin, H., & Tucker, D. 2009, ApJ, 696, L61
Kubo, J. M., Allam, S. S., Drabek, E., Lin, H., Tucker, D., Buckley-Geer, E. J., Diehl, H. T., Soares-Santos, M., Hao, J., Wiesner, M., West, A., Kubik, D., Annis, J., & Frieman, J. A. 2010, ApJ, 724, L137
Land, K., Slosar, A., Lintott, C., Andreescu, D., Bamford, S., Murray, P., Nichol, R., Raddick, M. J., Schawinski, K., Szalay, A., Thomas, D., & Vandenberg, J. 2008, MNRAS, 388, 1686
Limousin, M., Cabanac, R., Gavazzi, R., Kneib, J.-P., Motta, V., Richard, J., Thanjavur, K., Foex, G., Pello, R., Crampton, D., Faure, C., Fort, B., Jullo, E., Marshall, P., Mellier, Y., More, A., Soucail, G., Suyu, S., Swinbank, M., Sygnet, J.-F., Tu, H., Valls-Gabaud, D., Verdugo, T., & Willis, J. 2009, A&A, 502, 445
Limousin, M., Richard, J., Kneib, J.-P., Brink, H., Pelló, R., Jullo, E., Tu, H., Sommer-Larsen, J., Egami, E., Michałowski, M. J., Cabanac, R., & Stark, D. P. 2008, A&A, 489, 23
Lin, H., Buckley-Geer, E., Allam, S. S., Tucker, D. L., Diehl, H. T., Kubik, D., Kubo, J. M., Annis, J., Frieman, J. A., Oguri, M., & Inada, N. 2009, ApJ, 699, 1242
Lintott, C. J., Schawinski, K., Slosar, A., Land, K., Bamford, S., Thomas, D., Raddick, M. J., Nichol, R. C., Szalay, A., Andreescu, D., Murray, P., & Vandenberg, J. 2008, MNRAS, 389, 1179
LSST Science Collaborations, Abell, P. A., Allison, J., Anderson, S. F., Andrew, J. R., Angel, J. R. P., Armus, L., Arnett, D., Asztalos, S. J., Axelrod, T. S., & et al. 2009, ArXiv e-prints
Marshall, P. J., Hogg, D. W., Moustakas, L. A., Fassnacht, C. D., Bradač, M., Schrabback, T., & Blandford, R. D. 2009, ApJ, 694, 924
Marshall, P. J., et al. 2007, ApJ, 671, 1196
Moustakas, L. A., et al. 2007, ApJ, 660, L31
Newbury, P. R., & Spiteri, R. J. 2002, SIAM, 44, 111
Ofek, E. O., Seitz, S., & Klein, F. 2008, MNRAS, 389, 311
Oguri, M., & Marshall, P. J. 2010, MNRAS, 405, 2579
Orban de Xivry, G., & Marshall, P. 2009, MNRAS, 399, 2
Pettini, M., Christensen, L., D'Odorico, S., Belokurov, V., Evans, N. W., Hewett, P. C., Koposov, S., Mason, E., & Vernet, J. 2010, MNRAS, 402, 2335
Pettini, M., Rix, S. A., Steidel, C. C., Hunt, M. P., Shapley, A. E., & Adelberger, K. L. 2002, Ap&SS, 281, 461
Raddick, M. J., Bracey, G., Gay, P. L., Lintott, C. J., Murray, P., Schawinski, K., Szalay, A. S., & Vandenberg, J. 2010, Astronomy Education Review, 9, 010103
Sand, D. J., Treu, T., Ellis, R. S., & Smith, G. P. 2005, ApJ, 627, 32
Schneider, P., Kochanek, C. S., & Wambsganss, J. 2006, Gravitational Lensing: Strong, Weak & Micro (Lecture Notes of the 33rd Saas-Fee Advanced Course, Springer-Verlag: Berlin)
Smith, G. P., Kneib, J., Ebeling, H., Czoske, O., & Smail, I. 2001, ApJ, 552, 493
Spiniello, C., Koopmans, L. V. E., Trager, S. C., Czoske, O., & Treu, T. 2011, ArXiv e-prints
Stark, D. P., Ellis, R. S., Richard, J., Kneib, J., Smith, G. P., & Santos, M. R. 2007, ApJ, 663, 10
Stark, D. P., Swinbank, A. M., Ellis, R. S., Dye, S., Smail, I. R., & Richard, J. 2008, Nature, 455, 775
Swinbank, A. M., Webb, T. M., Richard, J., Bower, R. G., Ellis, R. S., Illingworth, G., Jones, T., Kriek, M., Smail, I., Stark, D. P., & van Dokkum, P. 2009, MNRAS, 400, 1121
Vegetti, S., & Koopmans, L. V. E. 2009, MNRAS, 392, 945
Wallin, J., Holincheck, A., Borne, K., Lintott, C., Smith, A., Bamford, S., & Fortson, L. 2010, in Astronomical Society of the Pacific Conference Series, Vol. 423, Astronomical Society of the Pacific Conference Series, ed. B. Smith, J. Higdon, S. Higdon, & N. Bastian, 217
Walsh, D., Carswell, R. F., & Weymann, R. J. 1979, Nature, 279, 381

APPENDIX

SINGULAR ISOTHERMAL ELLIPSOID GRAVITATIONAL LENS MODELS

An singular isothermal sphere has a projected mass distribution Σ that decreases with projected radius R as $\Sigma \propto R^{-1}$. Scaling the surface density Σ by the critical density gives the convergence $\kappa = \theta_{\rm Ein}/2\theta$, where $\theta_{\rm Ein}$ is the Einstein radius of the lens in angular units. The deflection angle is such that the vector lens equation, that describes the mapping from image to source plane, is then:

$$\boldsymbol{\beta} = \boldsymbol{\theta} - \hat{\boldsymbol{\theta}}, \tag{A1}$$

where $\hat{\boldsymbol{\theta}} = \boldsymbol{\theta}/|\boldsymbol{\theta}|$ is a unit vector in the direction of $\boldsymbol{\theta}$. The Einstein radius is related to the velocity dispersion parameter of this lens model, $\sigma_{\rm SIE}$, by

$$\theta_{\rm Ein} = 4\pi \left(\frac{\sigma_{\rm SIE}}{c}\right)^2 \frac{D_{\rm ds}}{D_{\rm s}}, \tag{A2}$$

where $D_{\rm ds}$ and $D_{\rm s}$ are the angular diameter distances between the lens and the source, and between us and the source, respectively.

The lens equation for an elliptically-symmetric isothermal mass distribution (an SIE model) was worked out by Kormann et al. (1994):

$$\boldsymbol{\beta} = \boldsymbol{\theta} - \theta_{\rm Ein}\frac{\sqrt{q}}{p}\left[\text{arcsinh}\left(\frac{p}{q}\cos(\phi)\right)\hat{\boldsymbol{\theta}}_x + \arcsin\left(p\sin(\phi)\right)\hat{\boldsymbol{\theta}}_y\right]. \tag{A3}$$

Here, q is the axis ratio of the ellipsoid in projection, $p = \sqrt{1-q^2}$, $\hat{\boldsymbol{\theta}}_x$ and $\hat{\boldsymbol{\theta}}_y$ are unit vectors and ϕ is the polar coordinate angle.

To calculate the deflection angle due to a collection of SIE components, we use the linearity of the lens equation and sum the deflections due to each component:

$$\boldsymbol{\beta} = \boldsymbol{\theta} - \boldsymbol{\alpha}_1(\boldsymbol{\theta}) - \boldsymbol{\alpha}_2(\boldsymbol{\theta}) - \ldots, \tag{A4}$$

and so on.

CRITICAL CURVES AND CAUSTICS

In addition to solving the lens equation, we need to compute the critical curves and caustics of the system. The critical curve is determined by the path where the magnification becomes infinite. The magnification μ at a particular point in the image plane is given by

$$\mu(\boldsymbol{\theta}) = \frac{1}{\left(1-\kappa(\boldsymbol{\theta})\right)^2 - |\gamma(\boldsymbol{\theta})|^2}, \tag{B1}$$

where κ and γ are the convergence and complex shear of the lens. Expressions for these quantities in the SIE model are given by Kormann et al. (1994). Here we note that for a collection of SIE lens components, the convergence and shear sum linearly, and the magnification can then be computed from the totals.

Numerically, we consider all points where the magnification exceeds 100 as approximating the critical curve. Having located a set of points in the image plane satisfying this criterion – by contour-following, for example – we then map the critical curve back to the source plane point by point using the lens equation. The result is the caustic curve.

TYPICAL STEPS TAKEN WHEN USING MOWGLI

With reference to the screenshot in Figure 0, we now describe the typical sequence of steps we found it helpful to take when modeling a simple, single-component lens candidate:

1. Mask out the lens and any foreground or background artifacts, by placing circular masks on the data image panel in "mask" view, and then adjusting their position, ellipticity and orientation to remove as much non-lensed light as possible, while preserving the lensed source features.

2. Add a circular lens at the center of the lens light distribution, in the "model" view of the data image panel.

3. Add a source at the center of the lens, in the right-hand predicted image panel. Note that the initial predicted image will be close to a complete Einstein ring.

4. Vary the Einstein radius of the lens until all the arcs are equidistant from the Einstein ring, with half the arcs inside the ring and half outside.

5. Slowly vary the ellipticity and orientation of the lens; at each step, quickly move the source around over the caustics to get an overview of the possible image configurations. The predicted image updates in real-time to allow rapid learning in this way. This is where the caustics display is most helpful, since the caustics define the natural coordinate system for the source position. Stop when the appropriate number of arcs are obtained in roughly the right positions.

6. Once the morphology of the arcs have been matched, it is then generally best to mask out areas of extraneous noise. This is done to assist MOWGLI in finding the ideal color of the predicted image, which will yield a more accurate $\hat{\chi}^2$ value. From this point onwards, it is worth paying close attention to the Ω value, since the visual impression of goodness of fit may not change very much.

7. Continue to vary the lens shape and source position as above. If needed, adjust the source ellipticity and orientation to refine the model.

Although some multiple-component lens models are significantly more complicated than any of the single-lens models, the basic steps needed to be taken to model these systems with MOWGLI are roughly the same. The steps which do differ from the single-lens method are as follows:

1. Place circular lenses at the centers of each of the proposed lens galaxy light distributions. While it is a good idea to try and model the lens with as few lens components, some image morphologies simply cannot be reproduced with simple models. We find that selecting the brightest red galaxies in the image, and associating mass with each of them, allows the arcs to be predicted more quickly than if a single mass distribution is used as the starting point. It is important to assign proportionately more mass to the brighter lens galaxies, at least at first.

2. Place a source at a position which produce images in the same general direction as the images which appear in the astronomical image – when the caustic structure is complex, moving the source around quickly is especially useful, and gives a good overview of which image configurations are possible.

3. Vary the lens ellipticities and orientations. This step involves a lot of trial and error, and can require patience. Again, the goal at this stage is to get the positions of the predicted arcs right: pay attention to lens galaxy configurations which move the arcs closer to their desired positions.

4. Adjust the source positions, seeking to optimize the arc positions and shapes. Often, the lenses must be slightly adjusted as the source is moved in order that one arc may be positioned without drastically affecting the remaining arcs. Pay special attention to the lens closest to the arc being positioned.